Remote Sensing of Environment 159 (2015) 134–151

Contents lists available at ScienceDirect

Remote Sensing of Environment

journal homepage: www.elsevier.com/locate/rse

Hyperspectral optical discrimination of phytoplankton community structure in Funka Bay and its implications for ocean color remote sensing of diatoms

Tomonori Isada [a,*], Toru Hirawake [a], Tsukuru Kobayashi [a], Yuichi Nosaka [b], Masafumi Natsuike [a], Ichiro Imai [a], Koji Suzuki [b,c], Sei-Ichi Saitoh [a]

[a] Faculty of Fisheries Sciences, Hokkaido University, 3-1-1 Minato-cho, Hakodate, Hokkaido 041-0821, Japan
[b] Graduate School of Environmental Science, Hokkaido University, North 10 West 5, Kita-ku, Sapporo, Hokkaido 060-0810, Japan
[c] Faculty of Environmental Earth Science, Hokkaido University, North 10 West 5, Kita-ku, Sapporo, Hokkaido 060-0810, Japan

ARTICLE INFO

Article history:
Received 26 December 2013
Received in revised form 8 December 2014
Accepted 8 December 2014
Available online 29 December 2014

Keywords:
Phytoplankton pigments
Light absorption
Derivative spectroscopy/similarity index
CHEMTAX
Hyperspectral remote sensing

ABSTRACT

Identification of phytoplankton functional groups is key to understanding marine biogeochemical cycles. For more accurate understanding of phytoplankton community structure and its implications for ocean color remote sensing applications, we investigated seasonal changes in phytoplankton pigments with high-performance liquid chromatography (HPLC), hyperspectral absorption coefficients of detritus ($a_d(\lambda)$), phytoplankton ($a_{ph}(\lambda)$), and colored dissolved organic matter ($a_{CDOM}(\lambda)$), and hyperspectral $a_{ph}(\lambda)$ derived from remote sensing reflectance ($a_{ph\_Rrs\text{-}derived}(\lambda)$) in the coastal waters of Funka Bay from 2010 to 2012. Chlorophyll *a* (Chl *a*) concentrations measured by HPLC ranged from 0.29 to 8.6 mg m^{-3}. Phytoplankton community compositions, as estimated by chemotaxonomic analysis (CHEMTAX) based on HPLC phytoplankton pigments, showed a seasonal succession of diatoms, chlorophyll *b*-containing phytoplankton (chlorophytes and prasinophytes), and cyanobacteria. Additionally, to identify the dominant type of phytoplankton with an alternative technique to CHEMTAX analysis, we employed a derivative spectroscopy/similarity index (SI) approach for $a_{ph}(\lambda)$ as an optical detection technique for discriminating between different types of phytoplankton. In particular for diatom-dominated stations, SI values relative to the second derivative spectra of $a_{ph}(\lambda)$ of diatom cultures, isolated from our study region, were significantly higher than those for chlorophyll *b*-containing phytoplankton- and cyanobacteria-dominated stations. Furthermore, we found a strong relationship between the SI values calculated from the second derivative spectra and the composition of diatoms as estimated by CHEMTAX. These results suggest that the two different methods validated each other's performance and precision in estimating relative diatom abundance from bulk samples and that it is possible to optically discriminate the dominance of diatoms using derivative spectra of $a_{ph}(\lambda)$. We extended this combination approach to hyperspectral $a_{ph\_Rrs\text{-}derived}(\lambda)$, using a quasi-analytical algorithm within 400–546 nm range. We found a significant correlation between SI values obtained from the second derivative spectra of $a_{ph\_Rrs\text{-}derived}(\lambda)/a_{ph\_Rrs\text{-}derived}(443)$ and the composition of diatoms derived by CHEMTAX, but it was not as high as for $a_{ph}(\lambda)$ measured by filter-pad analysis. These results indicate that using hyperspectral optical data of $a_{ph}(\lambda)$ and $R_{rs}(\lambda)$ with derivative spectroscopy is potentially a promising approach to identify seasonal variability in the composition of diatoms in coastal waters. Furthermore, a hyperspectral approach in combination with CHEMTAX analysis as a reference for phytoplankton community structure has proven useful in improving our understanding of phytoplankton community structure in the coastal waters of Funka Bay.

© 2014 Elsevier Inc. All rights reserved.

1. Introduction

Phytoplankton play a central role as carbon fixers in aquatic ecosystems. Although all phytoplankton utilize CO_2 to produce organic matter, some different taxonomic groups have unique physiological processes, which in turn affect marine biogeochemical cycles. For example, diatoms utilize silicates and are important bloom-forming phytoplankton, contributing ~40% of global ocean productivity (Armbrust, 2009; Falkowski, Barber, & Smetcek, 1998). In contrast, small cells such as cyanobacteria contribute to phytoplankton biomass and both primary and export production in oligotrophic waters (Richardson & Jackson, 2007). In coastal waters, phytoplankton contribute largely not only to the aquatic carbon cycle but also to aquaculture. It is well known that

* Corresponding author at: Akkeshi Marine Station, Field Science Center for Northern Biosphere, Hokkaido University, Aikappu 1, Akkeshi-cyo, Akkeshi-gun, Hokkaido 088-1113, Japan.
E-mail address: t-isada@fsc.hokudai.ac.jp (T. Isada).

http://dx.doi.org/10.1016/j.rse.2014.12.006
0034-4257/© 2014 Elsevier Inc. All rights reserved.

diatoms (e.g., *Pseudo-nitzschia* spp.), as well as harmful algae such as raphidophytes and dinoflagellates, influence cultured aquatic organisms, leading to concerns for both fishery markets and human health (Babin et al., 2005; Imai, Yamaguchi, & Hori, 2006). Therefore, it is essential to quantify and monitor phytoplankton community structure to understand the contribution of each phytoplankton group to marine biogeochemical cycles and their influence on cultured aquatic organisms.

Although several methods exist for identifying phytoplankton groups (e.g., microscopy, flow cytometry, and genetic analysis), phytoplankton pigment chemotaxonomy with high performance liquid chromatography (HPLC) is the most widely adopted method for estimating phytoplankton biomass and community structure (Kozlowski, Deutschman, Garibotti, Trees, & Vernet, 2011; Llewellyn, Fishwick, & Blackford, 2005). Phytoplankton pigments are also increasingly essential for recognizing phytoplankton functional types through satellite ocean color remote sensing (e.g., Alvain, Moulin, Dandonneau, & Bréon, 2005; Hirata et al., 2011; Pan, Mannino, Russ, Hooker, & Harding, 2010). For estimating phytoplankton community structure, the CHEMTAX program based on matrix factorization (Mackey, Mackey, Higgins, & Wright, 1996) is recognized as a useful and reliable tool. This program has been applied to various geographic domains, including the open ocean (e.g., Veldhuis & Kraay, 2004), iron fertilization experiments (e.g., Suzuki et al., 2005), and coastal waters (e.g., Isada et al., 2009). CHEMTAX has also been applied to satellite ocean color remote sensing (Pan, Mannino, Marshall, Filippino, & Mulholland, 2011). The program uses factor analysis and a steepest-descent algorithm to optimize the relative ratios of pigment:chlorophyll *a* (Chl *a*) used in calculating the abundance of each phytoplankton group contributing to Chl *a* concentration (Mackey et al., 1996). Therefore, the initial ratio matrix of pigment:Chl *a* influences the program's output of phytoplankton abundances. However, one of the major difficulties of the CHEMTAX program is the choice of an initial ratio matrix of pigment:Chl *a*, which is required to find the optimal ratio (Latasa, 2007; Wright et al., 2009).

Change in pigment composition is one of the major factors influencing the light absorption coefficient of phytoplankton, $a_{ph}(\lambda)$ (Bricaud, Claustre, Ras, & Oubelkheir, 2004; Hoepffner & Sathyendranath, 1991). Variations in $a_{ph}(\lambda)$ also depend on variations in the package effect (Morel & Bricaud, 1981), the size structures of phytoplankton (Ciotti, Lewis, & Cullen, 2002), light (Fujiki & Taguchi, 2002), and nutrients (Matsuoka, Larouche, Poulin, Vincent, & Hattori, 2009). Therefore, currently, $a_{ph}(\lambda)$ is used as an indicator of phytoplankton physiology and primary productivity (Hirawake, Shinmyo, Fujiwara, & Saitoh, 2012; Isada et al., 2013; Marra, Trees, & O'Reilly, 2007). Variations in $a_{ph}(\lambda)$ influence the light in the water column and, in turn, affect reflectance. Therefore, optical observations, including observations from in situ moored systems and ocean color remote sensing, are an effective tool for monitoring variability in phytoplankton dynamics in aquatic ecosystems (Cullen, Ciotti, Davis, & Lewis, 1997; Schofield et al., 1999). Derivative spectroscopy provides more detailed information on the spectral shape of $a_{ph}(\lambda)$ (Bidigare, Morrow, & Kiefer, 1989; Butler & Hopkins, 1970a,b; Faust & Norris, 1985; Millie, Kirkpatrick, & Vinyard, 1995; Smith & Alberte, 1994). This analysis amplifies minor inflections in the absorption spectrum and separates closely related pigments features. In this sense, several studies have investigated the relationship between photosynthetic pigments or species-specific pigments and the derivative spectra of $a_{ph}(\lambda)$ at a given wavelength in order to develop algorithms for retrieving phytoplankton pigments (Aguirre-gómez, Weeks, & Boxall, 2001; Astoreca et al., 2009). Based on derivative analysis, Millie et al. (1997) showed a method for detecting the toxic dinoflagellate *Karenia brevis* (formerly known as *Gymnodinium breve*) using the similarity index (SI), calculated by comparing the fourth derivative absorption spectra of an unknown sample with those of a reference monospecific *K. brevis* culture in laboratory experiments. Subsequently, Kirkpatrick, Millie, Moline, and Schofield (2000) demonstrated a linear relationship between *K. brevis* biomass and SI values in natural mixed populations. Thus, the derivative spectroscopy/similarity index (SI) approach for $a_{ph}(\lambda)$ would provide useful information to distinguish among phytoplankton groups, and potentially among species.

Recently, improvements have led to bio-optical hyperspectral sensors that become powerful tools for investigating phytoplankton dynamics in more detail (Chang et al., 2004; Devred et al., 2013; Ryan, Davis, Tufillaro, Kudela, & Gao, 2014). Highly resolved spectra of reflectance allow the discrimination of several distinguishing features related to the pigments and fluorescence of phytoplankton. Therefore, hyperspectral measurements of phytoplankton absorption ($a_{ph}(\lambda)$) and remote sensing reflectance ($R_{rs}(\lambda)$) with derivative spectroscopy have been exploited for use in various estimations such as seafloor types in carbonate sediments with microbial pigments (e.g., Louchard et al., 2002), seagrass and benthic algae (Dierssen, Zimmerman, Drake, & Burdige, 2010), phytoplankton pigment assemblages in open ocean (Torrecilla, Stramski, Reynolds, Millán-Núñez, & Piera, 2011), bio-optical provinces (Taylor et al., 2011), and phytoplankton size structure (Organelli, Bricaud, Antoine, & Uitz, 2013). Craig et al. (2006) developed a method for detecting *Karenia brevis* using hyperspectral $R_{rs}(\lambda)$ with a quasi-analytical algorithm (QAA, Lee & Carder, 2004), which is the inversion method for estimating $a_{ph}(\lambda)$. In this study, a derivative spectroscopy/SI approach for $a_{ph}(\lambda)$ was employed. Similarly, Lubac et al. (2008) assessed the suitability of multispectral and hyperspectral approaches for identifying *Phaeocystis globosa* blooms using field measurements of $R_{rs}(\lambda)$. They showed the advantage of a hyperspectral approach based on a derivative spectroscopy/SI analysis over a multispectral approach to detect different phytoplankton taxonomic groups with remote sensing.

The hyperspectral $a_{ph}(\lambda)$ data with the derivative spectroscopy/SI approach has been proven appropriate for discriminating among phytoplankton groups. However, extracting information on specific phytoplankton groups from $a_{ph}(\lambda)$ still remains a challenging task. In this sense, the use of CHEMTAX analysis based on HPLC phytoplankton pigments in natural waters can contribute to the investigation of the relationship between phytoplankton community structure and bulk optical absorption properties. An assessment of phytoplankton community structure and its relation to the light absorption of phytoplankton could improve our ability to use ocean optics and ocean color remote sensing to predict primary productivity and biogeochemical cycling.

The objective of this study is to investigate the utility of hyperspectral optical data for assessing the variability of phytoplankton groups using CHEMTAX analysis as a reference for phytoplankton community structure and also improve our ability to obtain more accurate estimations of phytoplankton community composition via ocean color remote sensing. To achieve this goal, an in situ seasonal dataset of phytoplankton pigments, cell densities of diatoms, hyperspectral absorption coefficients of detritus, phytoplankton, and colored dissolved organic matter ($a_d(\lambda)$, $a_{ph}(\lambda)$, and $a_{CDOM}(\lambda)$), and hyperspectral $R_{rs}(\lambda)$ was collected in the coastal waters of Funka Bay, which is located off the southwest of Hokkaido Island, Japan. Funka Bay is known to be one of the most important aquaculture regions for scallops, which depend on phytoplankton biomass and composition as a food source (Baba, Sugawara, Nitta, Endou, & Miyazono, 2009). The growth of hanging cultured scallops in Funka Bay is influenced by the diatom blooms (Hashimoto, Ueno, Takahashi, Suzuki, & Itabashi, 2010). In particularly, a method for discriminating diatoms from other phytoplankton taxa using hyperspectral optical measurements is described.

2. Methods

2.1. In situ samples and data collection

Seawater sampling and radiometric measurements were conducted from onboard the T/S *Ushio* Maru and T/S *Oshoro* Maru from April 2010 to January 2012 in Funka Bay and the Tsugaru Strait, in the coastal waters off southwestern of Hokkaido, Japan (Fig. 1 and Table 1). Water

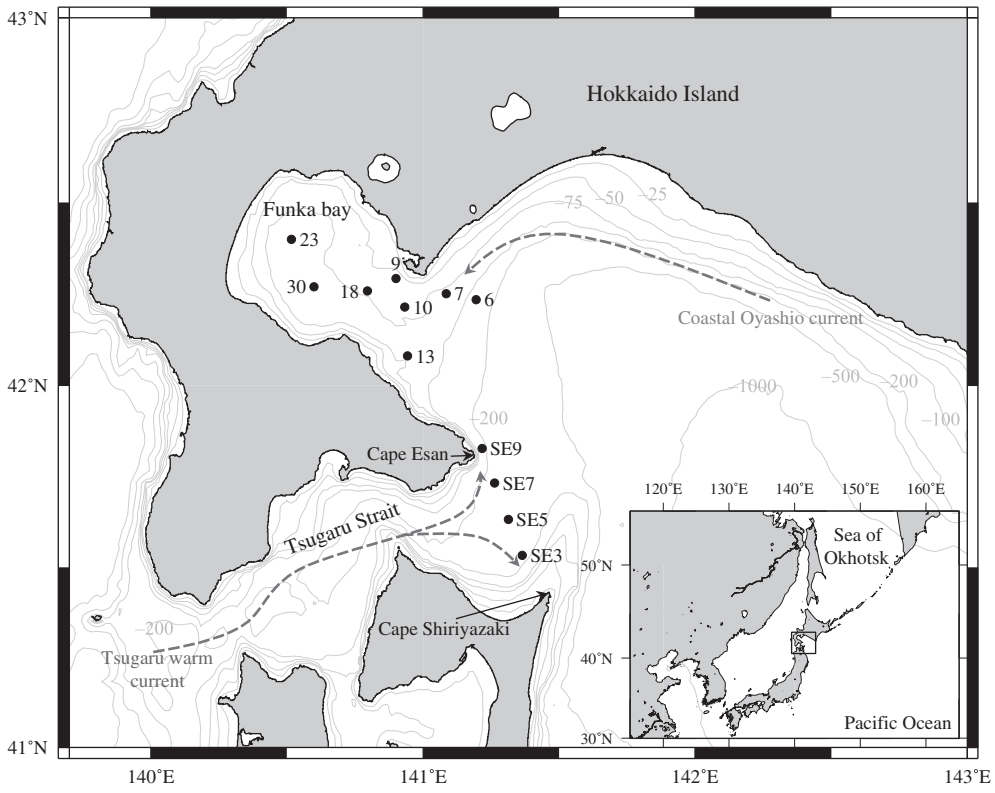

Fig. 1. Sampling stations in Funka Bay and the adjacent area in southern Hokkaido, Japan. The "S" and "E" in the eastern portion of Tsugaru Strait are the abbreviations of capes Shiriyazaki and Esan.

samples for phytoplankton pigments, cell densities of diatoms, light absorption properties (detritus, phytoplankton, and colored dissolved organic matter (CDOM)), and size-fractionated chlorophyll *a* concentrations were collected from surface waters (0–2 m) in acid-cleaned buckets and/or Niskin bottles attached to a CTD sampler (SBE 19plus Sea-Bird Electronics CTD) (Table 1).

2.2. Radiometric measurements and data processing of remote sensing reflectance

Vertical profiles of downwelling spectral irradiance, $E_d(\lambda)$, and upwelling radiance, $L_u(\lambda)$, were measured using a freefall hyperspectral profiling radiometer (HyperProII, Satlantic, Inc.). Incident irradiance at the sea surface, $E_{ds}(\lambda)$, was also measured. Measurements were taken over the spectral region 350–800 nm at a spectral resolution of 3.3 nm, with each band having a full-width half-maximum (FWHM) bandpass of 10 nm. Radiometers were operated at a distance of approximately 30–60 m from the vessel to avoid ship-shadow effects. Initial data processing for radiometric calibration, dark correction, immersion coefficient, pressure tare, data interpolation (0.1-m depth resolution), and the removal of data with tilt >5° was made using Prosoft v. 7.7.16 software (Satlantic, Inc.). No correction for sensor self-shading was applied. Next, each profile was visually checked and analyzed, and the depth intervals for the surface extrapolation were selected (mostly from 2–3 to 10 m). To avoid wave-focusing effects, data from measurements taken within the selected depth interval, generally starting

Table 1
A summary of sampling periods, number of stations, station names, and measurements conducted on each cruise in this study. US: *Ushio* Maru; OS: *Oshoro* Maru; Size-Chl *a*: size-fractionated chlorophyll *a* concentration by fluorometry; HPLC: phytoplankton pigments with HPLC; $a_{d,\,ph,\,CDOM}(\lambda)$: light absorption coefficients of detritus, phytoplankton, and colored dissolved organic matter (CDOM); $R_{rs}(\lambda)$: hyperspectral remote sensing reflectance; Cells: cell counting measurements by light microscopy.

Cruises	Periods	Total number of stations	Station names	Measurements
US194	19–21 April 2010	5	6, 9, 13, 23, 30	Size-Chl *a*, HPLC, $a_{d,\,ph,\,CDOM}(\lambda)$, $R_{rs}(\lambda)$
US196	21–23 May 2010	2	13, SE9	Size-Chl *a*, HPLC, $a_{d,\,ph,\,CDOM}(\lambda)$, $R_{rs}(\lambda)$
US199	19 June 2010	2	9, 13	Size-Chl *a*, HPLC, $a_{d,\,ph,\,CDOM}(\lambda)$, $R_{rs}(\lambda)$
US201	20–22 August 2010	3	9, 13, 30	Size-Chl *a*, HPLC, $a_{d,\,ph,\,CDOM}(\lambda)$, $R_{rs}(\lambda)$
US201-2	28–30 August 2010	2	13, SE9	Size-Chl *a*, HPLC, $a_{d,\,ph,\,CDOM}(\lambda)$, $R_{rs}(\lambda)$
US208	21–23 October 2010	2	13, 30	Size-Chl *a*, HPLC, $a_{d,\,ph,\,CDOM}(\lambda)$
US210	10–13 November 2010	2	13, SE9	Size-Chl *a*, HPLC, $a_{d,\,ph,\,CDOM}(\lambda)$
US219	6–8 February 2011	3	9, 13, 30	Size-Chl *a*, HPLC, $a_{d,\,ph,\,CDOM}(\lambda)$
OS225	21–25 February 2011	1	SE9	Size-Chl *a*, HPLC, $a_{d,\,ph,\,CDOM}(\lambda)$
US222	6 March 2011	1	13	Size-Chl *a*, HPLC, $a_{d,\,ph,\,CDOM}(\lambda)$, $R_{rs}(\lambda)$
US228	14–16 May 2011	7	7, 9, 13, 18, 23, 30, SE9	Size-Chl *a*, HPLC, $a_{d,\,ph,\,CDOM}(\lambda)$, Cells, $R_{rs}(\lambda)$
US232	27–28 July 2011	4	9, 13, SE3, SE9	Size-Chl *a*, HPLC, $a_{d,\,ph,\,CDOM}(\lambda)$, Cells, $R_{rs}(\lambda)$
US237	27–29 September 2011	8	7, 9, 10, 13, 18, 23, 30, SE9	Size-Chl *a*, HPLC, $a_{d,\,ph,\,CDOM}(\lambda)$, Cells, $R_{rs}(\lambda)$
US242	17–19 November 2011	4	13, SE3, SE5, SE9	Size-Chl *a*, HPLC, $a_{d,\,ph,\,CDOM}(\lambda)$, Cells
US246	10 January 2012	5	9, 10, 13, 18, 30	Size-Chl *a*, HPLC, $a_{d,\,ph,\,CDOM}(\lambda)$, Cells

at 2–3 m, were used. After that, the spectral diffuse attenuation coefficients for downwelling irradiance, $K_d(\lambda)$, and upwelling radiance, $K_{Lu}(\lambda)$, were determined as the slopes of least-squares regression fit of the log-transformed profiles of $E_d(\lambda)$ and $L_u(\lambda)$ (Stramski et al., 2008). Using the coefficients $K_d(\lambda)$ and $K_{Lu}(\lambda)$, values for $E_d(\lambda, z = 0^-)$, and $L_u(\lambda, z = 0^-)$ were calculated by extrapolating to beneath the sea surface. The spectral remote sensing reflectance just above the sea surface, $R_{rs}(\lambda)$, was calculated as follows:

$$L_w\left(\lambda, 0^+\right) = 0.544 \times L_u(\lambda, 0^-) \quad (1)$$

$$R_{rs}(\lambda) = \frac{L_w(\lambda, 0^+)}{E_{ds}(\lambda)}. \quad (2)$$

The coefficient 0.544 is the propagation factor for L_u at the air–sea interface (Austin, 1974; Mueller, Fargion, & McClain, 2003). In this study, $R_{rs}(\lambda)$ data observed under solar zenith angles over 60° with clouds were excluded. The angle values in the selected data ranged between 22° and 60° with a mean value of 44° ± 11°.

2.3. Phytoplankton pigments and size-fractionated chlorophyll a

The concentrations of chlorophylls and carotenoid pigments were measured with high-performance liquid chromatography (HPLC). Water samples (1000–2000 ml) were filtered onto Whatman GF/F filters (25-mm in diameter) under gentle vacuum pressure (<0.013 MPa). The filters were folded in half, blotted with filter paper, and immediately stored in liquid nitrogen before storage in a deep-freezer (−80 °C) until analysis on land. The frozen filters were broken into small pieces, soaked in 3 ml DMF (*N*,*N*-dimethylformamide) containing a known amount of canthaxanthin as an internal standard, and sonicated for 30 s on ice with a Branson SONIFIER model 250. The sample extract was filtered through 0.45-μm PTFE and mixed with a buffer solution of 28 mmol L^{-1} tetrabutylammonium acetate (TBAA) at pH 6.5. Then, the samples were kept at 4 °C for 5 min for equilibration before injection (Bidigare, van Heukelem, & Trees, 2005). The extracted samples were analyzed using a CLASS-VS HPLC system (Shimadzu) with a Zorbax Eclipse XDB-C8 150 × 4.6-mm internal diameter (ID) column with 3.5-μm particle size (Agilent Technologies), maintained at 60 °C. A binary linear gradient system proposed by Van Heukelem and Thomas (2001) was used to separate pigments by means of solvent A (28 mmol L^{-1} TBAA solution at pH 6.5: methanol, 30:70, v:v) and solvent B (100% methanol). Pigment separation was achieved within 30 min, including a binary linear gradient system with 5–95% B in 22 min, and an isocratic method with 95% B in 8 min. The flow rate was 1.2 mL min^{-1}. All pigment concentrations were calculated using response factors generated from calibration with a suite of pigment standards (DHI Water and Environment, Denmark).

The seawater samples (200–500 ml) for size-fractionated Chl *a* measurements by fluorometry were also filtered onto 47-mm Nuclepore membranes (10- or 2-μm pore size) or Whatman GF/F filters (~0.7-μm pore size) with a hand-operated vacuum pump (<0.013 MPa). The filters were soaked in 6 ml of DMF in a glass cuvette at −20 °C for more than 24 h (Suzuki & Ishimaru, 1990). Chl *a* concentration was determined using a Turner Designs 10-AU fluorometer with the non-acidification method of Welschmeyer (1994).

2.4. Cell densities of diatoms

The seawater samples (500 ml) for the identification and enumeration of diatom cell densities were preserved immediately with Lugol's iodine solution and refrigerated at 4 °C until counting in the laboratory on land. The samples were concentrated to 30 ml by setting, and aliquots of the concentrated samples were analyzed with an inverted microscope (NIKON ECLIPSE TE200). Identification of diatoms was carried out following Tomas (1997).

2.5. Light absorption coefficients of particles and CDOM

Water samples (1000–2000 ml) were filtered onto Whatman GF/F filters (25-mm in diameter) under gentle vacuum pressure (<0.013 MPa). The filters were immediately stored in liquid nitrogen until analysis on land. The optical density of all particles (OD_p) was measured every 1 nm from 350 to 750 nm using a multi-purpose spectrophotometer (MPS-2400 or MPS-2450, Shimadzu) equipped with an end-on type photomultiplier tube. The measurements were carried out according to the glass-fiber filter technique of Kishino, Takahashi, Okami, and Ichimura (1985). A blank filter wetted with filtered seawater was used as a blank. The particulate matter on the filter was soaked in NaClO solution (ca. 1% final concentration) to bleach phytoplankton pigments, according to Tassan and Ferrari (1995). The bleached filters were sufficiently rinsed by filtered seawater and measured to obtain the optical densities of detritus (OD_d). Both measured OD_p and OD_d were corrected for the path length amplification effect using the equation of Cleveland and Weidemann (1993) to convert them to hyperspectral absorption coefficients of particles and detritus, $a_p(\lambda)$ and $a_d(\lambda)$, respectively. The hyperspectral absorption coefficients of the phytoplankton, $a_{ph}(\lambda)$, were obtained by subtracting $a_d(\lambda)$ from $a_p(\lambda)$. Hereafter, the in situ light absorption spectra of phytoplankton obtained from filter-pad analysis are referred to as $a_{ph\_Filter\text{-}pad}(\lambda)$ when compared with $R_{rs}(\lambda)$-derived $a_{ph}(\lambda)$ by the inversion method (see Section 2.7.3).

For the measurement of absorption of colored dissolved organic matter (CDOM), seawater samples were filtered into glass bottles covered with aluminum foil using 47-mm Nuclepore membranes (0.2-μm pore size) with a hand-operated vacuum pump (<0.013 MPa). These filtered samples were then analyzed on board. The optical density of CDOM ($OD_{CDOM}(\lambda)$) was measured in a 10-cm quartz cylinder cell from 350 to 750 nm in 1-nm increments using a multi-purpose spectrophotometer (MPS-2400 or MPS-2450, Shimadzu) with reference to Milli-Q water. To minimize the effects of temperature and salinity on the absorbance among samples, the $OD_{CDOM}(\lambda)$ value averaged over a 5-nm interval around 685 nm was assumed to be 0, and the $OD_{CDOM}(\lambda)$ spectrum was shifted accordingly (Babin et al., 2003). Finally, the measured absorbance values were converted into hyperspectral absorption coefficients of CDOM, $a_{CDOM}(\lambda)$, by following the equation:

$$a_{CDOM}(\lambda) = 2.303 \frac{OD_{CDOM}(\lambda)}{0.1} \quad (3)$$

where 2.303 is a factor for converting between $\log_{10}$ and the natural logarithm, and 0.1 is the optical pathlength (m).

2.6. Diatom and dinoflagellate cultures

The $a_{ph}(\lambda)$ of three diatom species (*Thalassiosira nordenskioeldii*, *Chaetoceros debilis*, and *Chaetoceros furcellatus*) and one dinoflagellate species (*Alexandrium tamarense*), which were isolated from this study region, were measured to provide standard reference absorption spectra for diatoms and peridinin-containing dinoflagellates using the same methods described above (see Section 2.5). Each culture of the three diatom species was spiked with f/2 nutrients and maintained under a diel cycle of 13:11 h light:dark under 50 μmol photons m^{-2} s^{-1} 1 at 10 °C. *A. tamarense* was maintained under a diel cycle of 14:10 h light:dark under 100 μmol photons m^{-2} s^{-1} at 10 °C in modified SWM-3 media (Chen, Edelstein, & McLachlan, 1969; Imai, Itakura, Matsuyama, & Yamaguchi, 1996). In this study, exponentially growing cultures of diatoms and dinoflagellate were used. Additionally, the average light absorption coefficients of the three diatom species were used to represent the diatom group.

Table 2
Pigment to chlorophyll *a* ratios used for CHEMTAX in this study. (a) Seed ratio matrix derived from the work of [1]Isada et al. (2009), [2]Hashihama et al. (2008), [3]Higgins et al. (2011), and [4]Suzuki et al. (2005), (b) initial ratio matrix after 61 randomized starting matrices, and (c) final ratio matrix.

Name											
Class/pigment	Peri	19′-But	Fuco	Neo	Pras	Violax	19′-Hex	Allox	Zeax	Chl *b*	Chl *a*
(a) Seed ratio matrix											
Diatoms	0	0	0.66[1]	0	0	0	0	0	0	0	1
Dinoflagellates	0.89[1]	0	0	0	0	0	0	0	0	0	1
Haptophytes	0	0.005[3]	0.23[3]	0	0	0	1.25[2]	0	0	0	1
Pelagophytes	0	0.93[4]	0.62[4]	0	0	0	0	0	0	0	1
Cryptophytes	0	0	0	0	0	0	0	0.26[1]	0	0	1
Chlorophytes	0	0	0	0.066[3]	0	0.03[4]	0	0	0.06[4]	0.28[4]	1
Prasinophytes	0	0	0	0.063[3]	0.36[4]	0.11[4]	0	0	0.058[3]	0.89[4]	1
Cyanobacteria	0	0	0	0	0	0	0	0	0.33[4]	0	1
(b) Initial ratio matrix											
Diatoms	0	0	0.427	0	0	0	0	0	0	0	1
Dinoflagellates	0.847	0	0	0	0	0	0	0	0	0	1
Haptophytes	0	0.004	0.273	0	0	0	1.354	0	0	0	1
Pelagophytes	0	0.980	0.539	0	0	0	0	0	0	0	1
Cryptophytes	0	0	0	0	0	0	0	0.305	0	0	1
Chlorophytes	0	0	0	0.051	0	0.028	0	0	0.010	0.408	1
Prasinophytes	0	0	0	0.050	0.338	0.138	0	0	0.053	0.281	1
Cyanobacteria	0	0	0	0	0	0	0	0	0.375	0	1
(c) Final ratio matrix											
Diatoms	0	0	0.427	0	0	0	0	0	0	0	1
Dinoflagellates	0.847	0	0	0	0	0	0	0	0	0	1
Haptophytes	0	0.004	0.273	0	0	0	1.354	0	0	0	1
Pelagophytes	0	0.980	0.539	0	0	0	0	0	0	0	1
Cryptophytes	0	0	0	0	0	0	0	0.305	0	0	1
Chlorophytes	0	0	0	0.051	0	0.026	0	0	0.010	0.485	1
Prasinophytes	0	0	0	0.050	0.338	0.148	0	0	0.053	0.109	1
Cyanobacteria	0	0	0	0	0	0	0	0	0.375	0	1

Abbreviations: Peri, Peridinin; 19′-But, 19′-butanoyloxyfucxanthin; Fuco, fucoxanthin; Neo, neoxanthin; Pras, prasinoxanthin; Violax, violaxanthin; 19′-Hex, 19′-hexanoyloxyfucoxanthin; Allox, alloxanthin; Zeax, zeaxanthin; Chl *b*, chlorophyll *b*; Chl *a*, chlorophyll *a*.

2.7. Data analyses

2.7.1. Community composition of phytoplankton with the CHEMTAX program

Phytoplankton pigments data were used to calculate the contributions of various phytoplankton groups to the concentration of Chl *a* with CHEMTAX v1.95 (Mackey et al., 1996; Wright et al., 2009). The optimized marker pigment:Chl *a* ratios in this study region were determined following the method of multiple starting points for CHEMTAX optimization (Wright et al., 2009). Phytoplankton groups were selected based on previous studies with microscopy analysis in Funka Bay (Odate, 1989; Shinada, Shiga, & Ban, 1999; Tsunogai & Watanabe, 1983) and on Suzuki et al. (2005), who estimated the community composition of phytoplankton in the western subarctic Pacific. The seed pigment matrix was obtained from previous studies conducted in the northwest subarctic Pacific (Hashihama et al., 2008; Isada et al., 2009; Suzuki et al., 2005) and from Higgins, Wright, and Schlüter (2011) (see Table 2a). Next, 60 further pigment matrices were generated by the Microsoft Excel RAND function by multiplying a randomly determined factor F by each value in the seed pigment matrix, where $F = 1 + 0.7(R - 0.5)$, and R is a random number between 0 and 1. In total, 61 solutions were created. The best 10% of these solutions ($n = 6$) with the lowest root mean square errors provided by CHEMTAX were chosen and averaged as the optimized matrix (i.e., initial ratio matrix, Table 2b). Then, the final ratios were determined by CHEMTAX (Table 2c). By using CHEMTAX with the ratios, the following phytoplankton groups were distinguished: diatoms, dinoflagellates (type 1, Zapata, Fraga, Rodríguez, & Garrido, 2012), haptophytes (type 6, Zapata et al., 2004), pelagophytes, cryptophytes, chlorophytes, prasinophytes (type 3), and cyanobacteria.

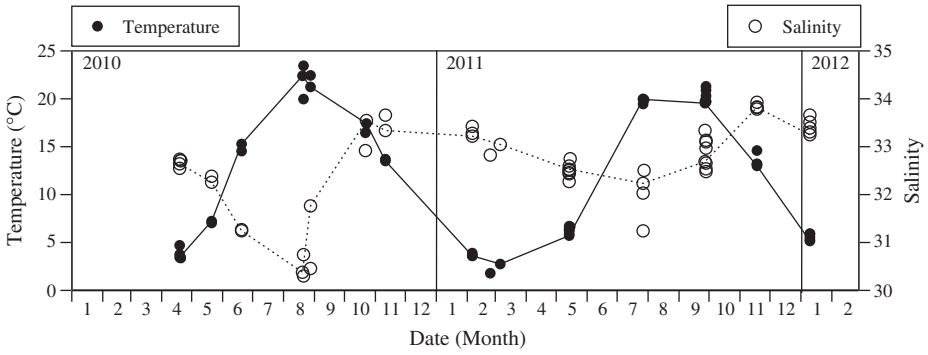

Fig. 2. Spatiotemporal variability in temperature and salinity measured by CTD at the surface (0–2 m) from April 2010 to January 2012.

Additionally, we applied a multiple linear regression analysis of the CHEMTAX-derived Chl *a* concentrations of each phytoplankton group to $a_{ph\_Filter\text{-}pad}(\lambda)$ data for several combinations of three bands in the Sea-viewing Wide Field-of-view Sensor (SeaWiFS), Moderate-resolution Imaging Spectroradiometer (MODIS), and MEdium Resolution Imaging Spectrometer (MERIS) following Sathyendranath et al. (2005) and the equation:

$$[\mathrm{Chl}a_{\_PFT}] = b_1\left[a_{ph\_Filter\text{-}pad}(\lambda_i)\right] + b_2\left[a_{ph\_Filter\text{-}pad}(\lambda_{i+1 \text{ or } i+2})\right] + b_3\left[a_{ph\_Filter\text{-}pad}(\lambda_{i+2 \text{ or } i+3})\right] \quad (4)$$

where [Chl $a_{\_PFT}$] is the CHEMTAX-derived Chl *a* concentration for the phytoplankton Functional types (PFTs): diatoms, Chl *b*-containing phytoplankton (chlorophytes plus prasinophytes), and cyanobacteria. b_1, b_2, and b_3 are partial regression coefficients, and *i* is the band number of ocean color sensors. The combinations of three bands considered in the analysis were as follows: 412–443–490, 443–490–510, 443–490–530, 490–510–555, and 490–530–555.

2.7.2. Cluster analysis based on HPLC phytoplankton pigments, CHEMTAX outputs, and hyperspectral optical data

A hierarchical cluster analysis was used to classify the seasonal dataset of phytoplankton pigments into specific pigment groups. Ratios of the concentration of each individual pigment to chlorophyll *a* levels were used to minimize the variability in pigment composition associated with changes in phytoplankton biomass and to account for differences in magnitude of these ratios in the cluster analysis (Pan et al., 2010; Taylor et al., 2011; Torrecilla et al., 2011). The pigments used in CHEMTAX analysis were employed for this analysis (Table 2). To select the most suitable clustering algorithm, five clustering algorithms (i.e., ward, single, complete, unweighted pair group method using arithmetic averages (UPGMA), and weighted pair group method using arithmetic averages (WPGMA)) with Euclidean distance were assessed following the method proposed by Mérigot et al. (2010) and Carteron, Jeanmougin, Leprieur, and Spatharis (2012). The results showed that UPGMA outperformed others in this study. Therefore, the cluster analysis based on HPLC pigments was carried out using Euclidian as a distance metric and UPGMA as a linkage algorithm. We also performed cluster analysis using CHEMTAX estimates based on Euclidian distance and UPGMA. Following Torrecilla et al. (2011) and Taylor et al. (2011), an angular distance was used for hyperspectral optical data of $a_{ph\_Filter\text{-}pad}(\lambda)$ because it reflects mainly the differences in the spectral shape of optical data. Next, the cophenetic index (*c*), a measure of how precisely two cluster trees preserve their structure between data objects, among these trees was calculated. It provides a measure of similarity between the absorption cluster trees and a reference cluster tree based on HPLC pigments. The analyses were conducted using R version 3.0.1 (R Development Core Team) with the clue (Hornik, 2012) and proxy (Meyer & Buchta, 2012) packages.

2.7.3. Inversion method of phytoplankton absorption spectra with hyperspectral $R_{rs}(\lambda)$

Light absorption spectra of phytoplankton were also derived from in situ hyperspectral $R_{rs}(\lambda)$ with the inversion method of Quasi-Analytical Algorithm (QAA) version 5 (Lee & Carder, 2004; Lee, Lubac, Werdell, & Arnone, 2009). Because it is difficult to derive $a_{ph}(\lambda)$ from $R_{rs}(\lambda)$ at wavelengths over 555 nm due to the strong dominance of pure water in the total absorption of this spectral region (Craig et al., 2006; Lee & Carder, 2004), data beyond this range were not used in this study. The root mean square error (RMSE), which was computed as relative values to give equal weights to all measurements, and the percentage difference (PD) were calculated to quantify differences in the spectra between $a_{ph\_Filter\text{-}pad}(\lambda)$ and $a_{ph\_Rrs\text{-}derived}(\lambda)$ using the following equations:

$$\mathrm{RMSE} = \sqrt{\frac{\sum_{i=1}^{n}\left[\log_{10}\left(a_{ph\_Rrs\text{-}derived}(\lambda)\right) - \log_{10}\left(a_{ph\_Filter\text{-}pad}(\lambda)\right)\right]^2}{n}} \quad (5)$$

$$\mathrm{PD} = \frac{\sqrt{\mathrm{mean}\left[a_{ph\_Filter\text{-}pad}(\lambda) - a_{ph\_Rrs\text{-}derived}(\lambda)\right]^2}}{\mathrm{mean}\left[a_{ph\_Filter\text{-}pad}(\lambda)\right]} \times 100\% \quad (6)$$

where *n* is the number of samples.

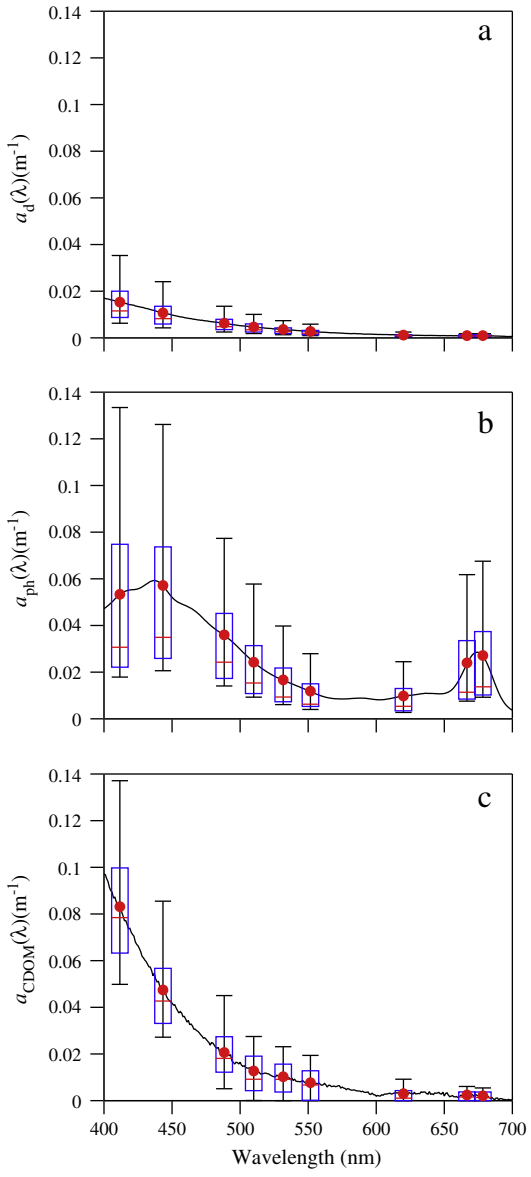

Fig. 3. Spectral averages observed in this study of the absorption coefficient of (a) detritus ($a_d(\lambda)$), (b) phytoplankton ($a_{ph}(\lambda)$), and (c) CDOM ($a_{CDOM}(\lambda)$). $a_d(\lambda)$ and $a_{ph}(\lambda)$ were determined by filter-pad analysis, and $a_{CDOM}(\lambda)$ by spectrophotometric measurement on board. Box plots of each absorption component correspond to MODIS (412, 443, 488, 531, 551, 667, and 678 nm), SeaWiFS (510 nm), and MERIS (510 and 620 nm) bands. Blue rectangles, red horizontal lines in boxes, red closed circles, and I-bars represent interquartile ranges, medians, means, and minimum and maximum values, respectively, except for outliers exceeding 1.5 times the interquartile ranges.

2.7.4. Derivative analysis and similarity index

Derivative analysis is helpful in the study of hyperspectral data (Tsai & Philpot, 1998), because it provides detailed information about small spectral variations. To investigate the similarities of both $a_{ph\_Filter\text{-}pad}(\lambda)$ and $a_{ph\_Rrs\text{-}derived}(\lambda)$ relative to the reference $a_{ph}(\lambda)$ phytoplankton cultures, derivative spectroscopy was applied to these spectra. Before the derivative analysis, $a_{ph}(\lambda)$ data were normalized to $a_{ph}(443)$ to emphasize the spectral shape of absorption rather than its magnitude. Additionally, a mean filter smoothing method to minimize some of the random noise was applied to the normalized spectra:

$$\overline{a}_{ph}\left(\lambda_j\right) = \frac{\sum_{i=1}^{n} a_{ph}(\lambda_i)/a_{ph}(443)}{n}, \tag{7}$$

where n is the filter size (FS) and j is the index of the middle point of the filter. Hereafter, the smoothed spectra of $a_{ph}(\lambda)/a_{ph}(443)$ are referred to as the non-derivative spectra.

After smoothing, the second derivative spectra (2^{nd} deriv.) of $a_{ph}(\lambda)/a_{ph}(443)$ were computed as follows (see Tsai & Philpot, 1998):

$$\left.\frac{d^2 a_{ph}}{d\lambda^2}\right|_j = \frac{\overline{a}_{ph}(\lambda_i) - 2\overline{a}_{ph}\left(\lambda_j\right) + \overline{a}_{ph}(\lambda_k)}{(\Delta\lambda)^2}, \tag{8}$$

where $\Delta\lambda$ ($=\lambda_k - \lambda_j = \lambda_j - \lambda_i$) is the band separation (BS) between adjacent bands. It is important to determine the suitable selection of FS and BS in the smoothing and derivative analysis. In this study, 9 nm was chosen for both FS and BS, according to the analysis performed by Torrecilla et al. (2011), in which the optimal values of FS and BS for hyperspectral $a_{ph}(\lambda)$ data were examined.

The non- and second derivative spectra of $a_{ph\_Filter\text{-}pad}(\lambda)/a_{ph\_Filter\text{-}pad}(443)$ and $a_{ph\_Rrs\text{-}derived}(\lambda)/a_{ph\_Rrs\text{-}derived}(443)$ were compared with those corresponding to the phytoplankton cultures using the similarity index (SI) as an angular distance (Kirkpatrick et al., 2000; Millie et al., 1997; Schofield et al., 1999):

$$SI = 1 - \frac{2}{\pi} \times \arccos\left(\frac{x_1 \cdot x_2}{\|x_1\| \times \|x_2\|}\right), \tag{9}$$

where x_1 includes the non- and second derivative spectra of phytoplankton cultures, and x_2 is the corresponding spectra of $a_{ph\_Filter\text{-}pad}(\lambda)/a_{ph\_Filter\text{-}pad}(443)$ or $a_{ph\_Rrs\text{-}derived}(\lambda)/a_{ph\_Rrs\text{-}derived}(443)$. The value of SI is a number from 0 to 1, and is equal to 1 when perfect similarity exists between the analyzed spectrum and the standard reference absorption spectrum of the phytoplankton culture. Regarding SI calculation, although the wavelength range used for the second derivative analysis using filter-pad analysis was 400–700 nm, the calculated wavelengths ranged from 409 ($=400+9$) to 691 ($=700-9$) nm. For R_{rs}-derived $a_{ph}(\lambda)$, wavelengths of 400–546 nm were used for the second derivative analysis, and the calculated wavelengths ranged from 409 ($=400+9$) to 537 ($=546-9$) nm (see Section 3.5).

3. Results

3.1. Physical properties and water mass classification from the absorption budget

Seasonal changes in seawater temperatures and salinities at the surface (0–2 m) from April 2010 to January 2012 are shown in Fig. 2. Water masses in April 2010 and from February to March 2011 were influenced by the intrusion of the Coastal Oyashio Water (COW) ($0 <$ temperature < 3 °C; $32.0 <$ salinity < 33.3; Miyake et al., 1988; Nakada et al., 2013). In particular, water masses in late February and March 2011 were completely occupied by the COW. After the intrusion of the COW, sea surface temperatures (SST) from May to August 2010 and from May to September 2011 gradually increased as the sea surface

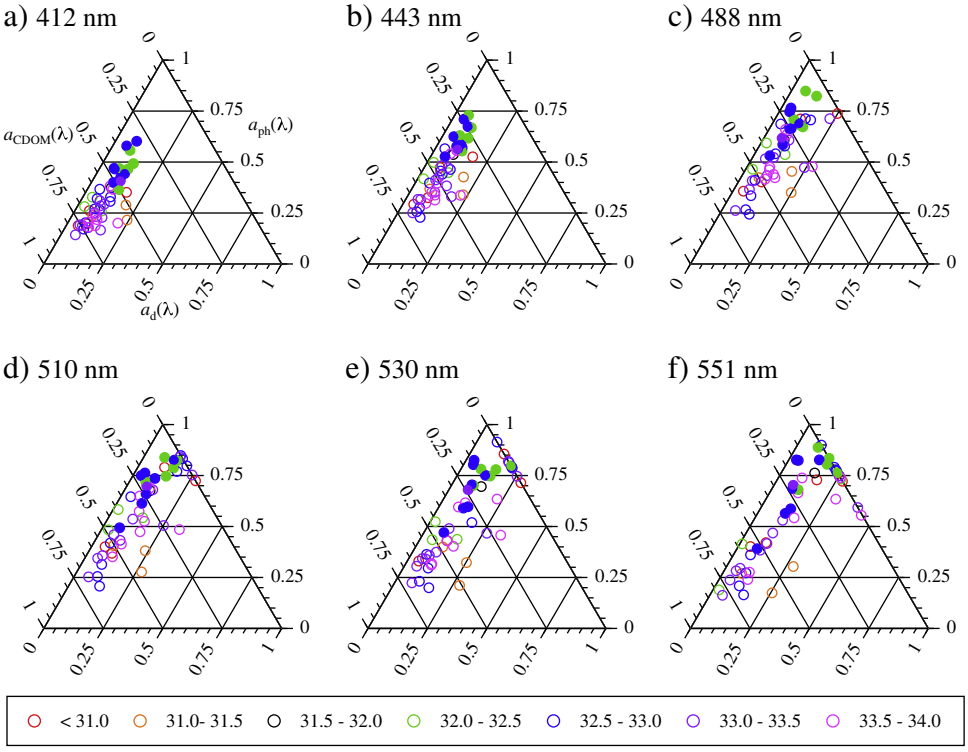

Fig. 4. Ternary plots of the relative absorption attributed to detritus, phytoplankton, and CDOM at different wavelengths corresponding to the MODIS, SeaWiFS, and MERIS bands. Each color represents a different range of salinity. Closed symbols in each color represent stations where chlorophyll a concentration was >2 mg m^{-3}.

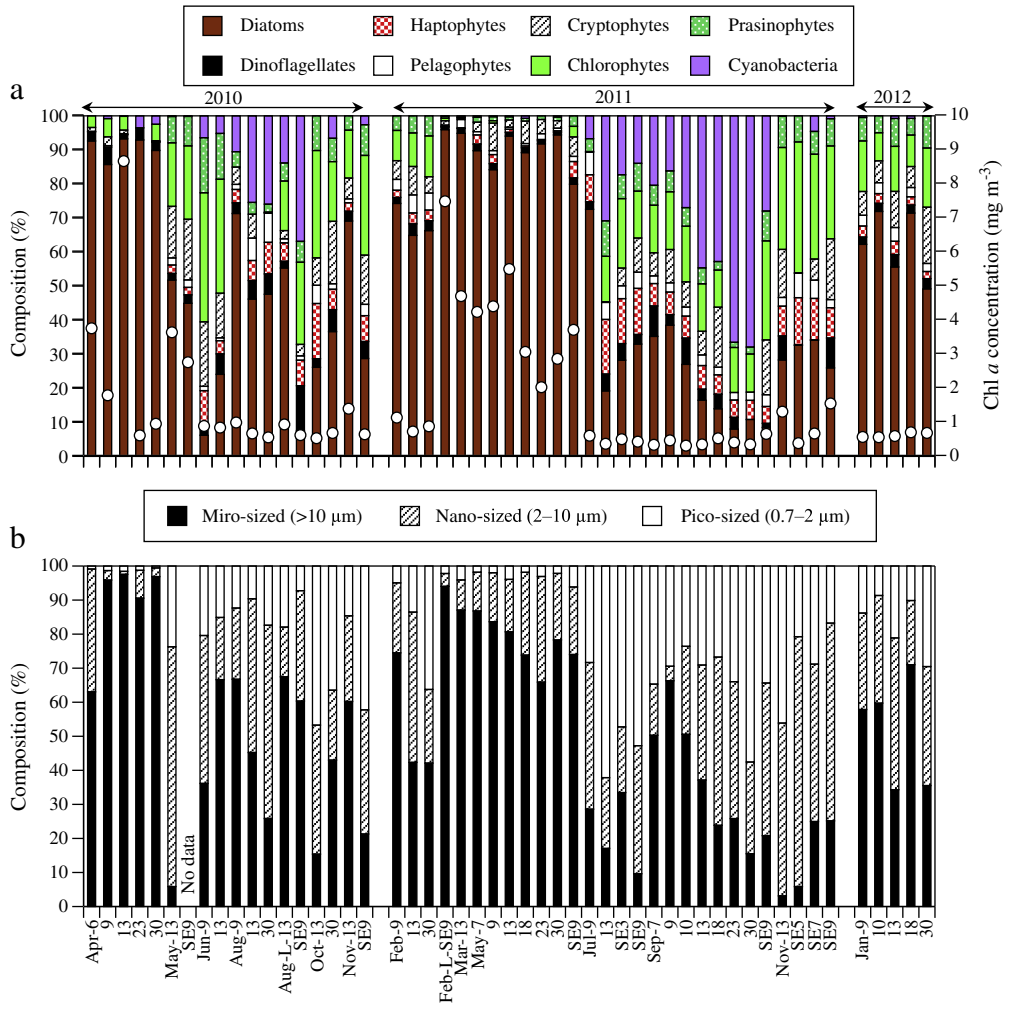

Fig. 5. (a) Contribution of each phytoplankton group to Chl *a* concentration, as estimated by CHEMTAX analysis, and (b) the relative contribution of each size fraction to total Chl *a* levels, determined fluorometrically at the surface. Open circles in (a) represent the Chl *a* concentrations measured by HPLC. The numbers in x-axis indicate station names.

decreased in salinity due to the effects of melting snow (Nakada et al., 2013). In October 2010 and November of both years, the water mass was influenced by the intrusion of the Tsugaru Warm Water, high saline water (T > 6 °C, salinity > 33.6), which originates from the Kuroshio (Kuroda et al., 2012). Subsequently, the surface water temperature gradually decreased toward January and February during winter. Thus, different types of water mass were encountered during each cruise.

Light absorption coefficients of detritus ($a_d(\lambda)$), phytoplankton ($a_{ph}(\lambda)$), and CDOM ($a_{CDOM}(\lambda)$) observed in this study are summarized in Fig. 3. The seasonal variability of $a_d(\lambda)$ was low when compared with $a_{ph}(\lambda)$ and $a_{CDOM}(\lambda)$. To characterize water masses in terms of the light absorption budget, the relative contributions of each absorption component to the total non-water absorption ($a_{t\text{-}w}(\lambda) = a_d(\lambda) + a_{ph}(\lambda) + a_{CDOM}(\lambda)$) were examined at wavelengths corresponding to MODIS bands and at the 510-nm wavelength of both SeaWiFS and MERIS (Fig. 4). Ternary plots of these three components showed that $a_{CDOM}(\lambda)$, especially at 412 and 443 nm, was the major light absorbing component, except for the spring phytoplankton bloom (when Chl *a* concentrations were >2.0 mg m^{-3}, see closed symbols in Fig. 4), and that the majority of $a_d(\lambda)$ was less than 25% at all wavelengths. These results were consistent with the previous research findings of Sasaki, Miyamura, Saitoh, and Ishizaka (2005) in Funka Bay. Values of $a_{CDOM}(\lambda)$ in this study were not significantly correlated with salinity except at 412 nm ($R = -0.32$, $p < 0.05$, $n = 51$).

3.2. Phytoplankton community compositions based on CHEMTAX and size-fractionated Chl a

Chlorophyll *a* (Chl *a*) concentrations measured by HPLC and phytoplankton community compositions as estimated from CHEMTAX

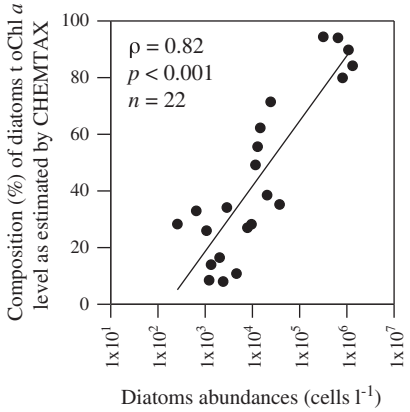

Fig. 6. Relationship between the composition of diatoms as estimated by CHEMTAX analysis and the cell densities of diatoms with microscopy from May 2011 to January 2012 (see Table 1).

analysis over the study period were shown in Fig. 5a. Chl *a* concentrations (closed white circles in Fig. 5a) varied by a factor of 30 and ranged from 0.29 mg m^{-3} at Stn. 10 in September 2011 to 8.6 mg m^{-3} at Stn. 13 in April 2010. The calculated pigment:Chl *a* ratios in CHEMTAX analysis (Table 2) were within the range of the values recently summarized by Higgins et al. (2011), except for the Chl *b*:Chl *a* ratio of prasinophytes. The Chl *b*:Chl *a* ratio of prasinophytes (0.109, Table 2c) in this study was slightly lower than the minimum values in the culture (0.131) of Higgins et al. (2011) but was within the range of 0.020–2.111, with an average of 0.911 ± 0.580, obtained from the field data of Higgins et al. (2011); see Table 6.2. As shown by CHEMTAX results (Fig. 5a), the composition of diatoms to Chl *a* levels varied widely over the study period, from 6 to 96%. A significant relationship between the composition of diatoms as estimated by CHEMTAX and the cell densities of diatoms from May 2011 to January 2012 was found in this study (Fig. 6 and Table 1). In particular, diatoms contributed >80% to Chl *a* concentrations during the spring bloom (April in 2010 and from February to May in 2011). Furthermore, winter populations in January 2012 and February 2011 mainly consisted of diatoms (ca. >50%). Chl *b*-containing phytoplankton (chlorophytes and prasinophytes) were widely distributed after the spring diatom blooms, in May and June 2010, and during autumn, in November 2011, and they were the secondary component during winter, in February 2011 and January 2012. The highest composition (54%) of summed chlorophytes and prasinophytes was found at Stn. 9 in June 2010. Cyanobacteria were the secondary and major constituents of the population in August 2010 and July and September 2011, respectively. Their contribution reached a maximum of 68% at Stn. 30 in September 2011. The compositions of haptophytes and cryptophytes were somewhat enhanced during summer and autumn. No predominance of dinoflagellates or pelagophytes was found over the study period. Micro-sized (>10 μm) phytoplankton estimated by fluorometry mainly dominated the phytoplankton community from January to May, when diatoms predominated, whereas nano- (2–10 μm) and pico-sized (0.7–2 μm) phytoplankton dominated the community during summer and autumn (Fig. 5b). According to these results, spearman's rank correlation test showed significant relationships among the compositions of micro-, nano-, and pico-sized Chl *a* by fluorometry; the CHEMTAX composition of diatoms plus dinoflagellates ($\rho = 0.77$, $p < 0.001$, $n = 50$), the sum of haptophytes, pelagophytes, and cryptophytes ($\rho = 0.65$, $p < 0.001$, $n = 50$), and the sum of chlorophytes, prasinophytes, and cyanobacteria ($\rho = 0.75$, $p < 0.001$, $n = 50$), respectively (Fig. 5).

The cluster analysis based on HPLC pigments mainly classified the seasonal pigments dataset into four cluster groups (Fig. 7). Average values for the ratios of each individual pigment concentration to Chl *a* levels and for the phytoplankton community composition as estimated by CHEMTAX in each cluster are shown in Table 3. These results show that the first and second clusters consisted of diatoms (Clusters A and B), the third cluster was dominated by cyanobacteria (Cluster C), and the fourth cluster contained predominantly Chl *b*-containing phytoplankton (i.e., chlorophytes and prasinophytes) or mixed phytoplankton populations (Cluster D). Additionally, although phytoplankton community structures were nearly the same within each cluster, Chl *a* concentrations considerably changed. The cophenetic index (*c*) between HPLC pigments- and CHEMTAX-based cluster trees was 0.539 (Table 4). This is most likely due to that HPLC pigments data is a direct approach to phytoplankton community characterization, whereas CHEMTAX has some uncertainties related to the initial ratio of pigment:Chl *a*. The compositions of diatoms as estimated by CHEMTAX were high in Clusters A and B (Fig. 5a), because the highest average value of pigment to Chl *a* ratio levels in Clusters A and B was the ratio of Fuco:Chl *a* (Table 3). However, the rest of pigment ratios in Cluster A differed from those in Cluster B, thereby leading to the separation of two stations in Cluster A from Cluster B. When two data in Cluster A (i.e., Stns. 6 and 23 in April

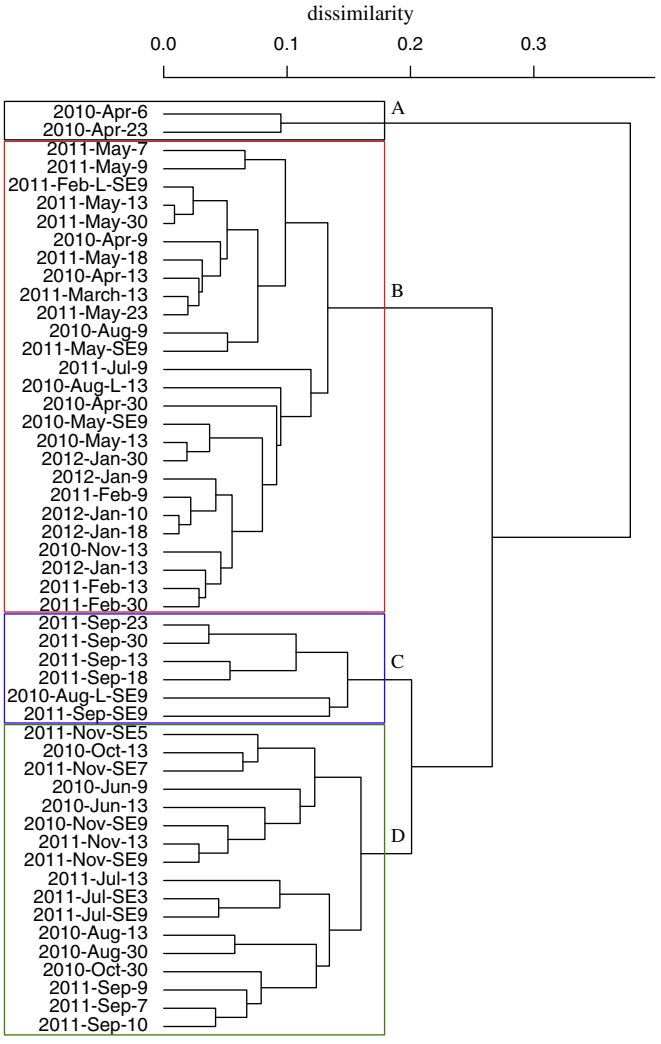

Fig. 7. Results of cluster analysis of phytoplankton pigments based on the Euclidean distance and UPGMA. Framed rectangles A, B, C, and D represent cluster groups.

Table 3
The average for the ratios of each pigment concentration to Chl *a* levels and for the phytoplankton composition as estimated by CHEMTAX, corresponding to each cluster based on phytoplankton pigments.

	Cluster			
	A $n = 2$ Mean ± SD	B $n = 26$ Mean ± SD	C $n = 6$ Mean ± SD	D $n = 17$ Mean ± SD
Phytoplankton pigment				
Peri	0.031 ± 0.004	0.018 ± 0.009	0.037 ± 0.042	0.041 ± 0.023
19′-But	0.001 ± 0.001	0.021 ± 0.016	0.025 ± 0.007	0.037 ± 0.020
Fuco	0.539 ± 0.064	0.333 ± 0.060	0.089 ± 0.018	0.157 ± 0.037
Neo	0.003 ± 0.002	0.006 ± 0.004	0.013 ± 0.005	0.016 ± 0.004
Pras	0.000 ± 0.000	0.012 ± 0.011	0.013 ± 0.010	0.026 ± 0.012
Violax	0.000 ± 0.000	0.007 ± 0.005	0.015 ± 0.007	0.018 ± 0.010
19′-Hex	0.000 ± 0.000	0.031 ± 0.026	0.082 ± 0.015	0.129 ± 0.049
Allox	0.003 ± 0.004	0.018 ± 0.015	0.023 ± 0.024	0.028 ± 0.019
Zeax	0.008 ± 0.011	0.008 ± 0.014	0.186 ± 0.059	0.050 ± 0.039
Chl *b*	0.011 ± 0.015	0.038 ± 0.037	0.089 ± 0.043	0.116 ± 0.053
Phytoplankton group				
Diatoms	92.8 ± 0.28	75.5 ± 15.9	10.9 ± 3.6	30.5 ± 9.7
Dinoflagellates	3.1 ± 0.6	2.2 ± 1.0	4.2 ± 4.7	4.8 ± 2.7
Haptophytes	0.0 ± 0.0	2.3 ± 1.9	6.0 ± 1.0	9.7 ± 3.8
Pelagophytes	0.1 ± 0.1	2.2 ± 1.7	2.5 ± 0.8	3.9 ± 2.2
Cryptophytes	0.6 ± 0.8	5.7 ± 4.8	7.3 ± 7.8	9.3 ± 6.2
Chlorophytes	1.7 ± 2.4	7.0 ± 6.9	17.1 ± 7.6	21.8 ± 11.8
Prasinophytes	0.0 ± 0.0	3.6 ± 3.0	4.3 ± 2.8	8.0 ± 3.4
Cyanobacteria	1.8 ± 2.5	1.5 ± 3.4	47.8 ± 16.1	12.0 ± 10.8

Table 4
The cophenetic indices (c) between pigment-, CHEMTAX-, and filter-pad $a_{ph}(\lambda)$-based cluster trees in the different wavelength ranges.

	HPLC	CHEMTAX
CHEMTAX	0.539	–
Filter-pad $a_{ph}(\lambda)$ (400–700 nm)		
Non-derivative spectra	0.197	0.056
2nd derivative spectra	0.318	0.410
Filter-pad $a_{ph}(\lambda)$ (400–546 nm)		
Non-derivative spectra	0.266	0.020
2nd derivative spectra	0.309	0.339

2010) were excluded, higher c value (0.727) between HPLC pigment- and CHEMTAX-based cluster trees was found compared with the c value using all data (0.539).

3.3. Phytoplankton absorptions and the derivative spectra of in situ measurements and cultures

Fig. 8 shows examples of the in situ phytoplankton absorption spectra normalized at 443 nm ($a_{ph\_Filter\text{-}pad}(\lambda)/a_{ph\_Filter\text{-}pad}(443)$) and their second derivative spectra (2nd deriv. of $a_{ph\_Filter\text{-}pad}(\lambda)/a_{ph\_Filter\text{-}pad}(443)$) among stations in which diatoms predominated (95%, Stn. 13 in March 2011 in Cluster B), Chl *b*-containing phytoplankton (54%, total of chlorophytes and prasinophytes, Stn. 9 in June 2010 in Cluster D), and cyanobacteria (68%, Stn. 30 in September 2011 in Cluster C) estimated by CHEMTAX. Although the non-derivative spectrum of chlorophytes seemed similar to that of cyanobacteria, the second derivative spectra of the two groups were distinct. At wavelengths between 400 and 550 nm, larger differences in the second derivative spectra were found among phytoplankton groups due to the different compositions of carotenoid pigments (Bricaud et al., 2004). Additionally, differences in the second derivative spectra of diatoms and either chlorophytes or cyanobacteria were also found at wavelengths over 555 nm. The c values of $a_{ph\_Filter\text{-}pad}(\lambda)$-based cluster tree relative to HPLC pigments- and CHEMTAX-based cluster trees were also calculated (Table 4). The c values were high when using second derivative spectra in two different ranges. However, smaller c values were obtained compared with the c value between HPLC pigments- and CHEMTAX-based cluster trees.

The absorptions and derivative spectra normalized at 443 nm of the average of the three diatom species, and the peridinin-containing dinoflagellate (*A. tamarense*) are shown in Fig. 9. The spectral shape of the three diatom average differed from the spectral shape of the dinoflagellate *A. tamarense* at all spectral ranges.

3.4. Similarity analysis of $a_{ph}(\lambda)$ of in situ measurements and cultures

Average SI values relative to $a_{ph}(\lambda)$ of the average of three diatom cultures and dinoflagellate culture using $a_{ph\_Filter\text{-}pad}(\lambda)$ data within the 400–700 nm range in each HPLC pigment-based cluster (Fig. 7) are summarized in Table 5. In terms of the average of three diatom cultures, SI values were clearly high in diatom-dominated stations (Clusters A and B) when considering second derivative spectra. Furthermore, the SI values estimated from the second derivative spectra were also highly correlated with the composition of diatoms as calculated from CHEMTAX (Spearman's rank correlation, Fig. 10a–b) and the cell densities of diatoms with microscopy (Spearman's rank correlation, Fig. 10c–d). In using the range of 400–546 nm, the highest Spearman's rank correlation between SI values and the composition of diatoms as estimated by CHEMTAX was found when using second derivative spectra (non-derivative spectra: $\rho = 0.13$, $p = 0.36$, $n = 51$; second derivative spectra: $\rho = 0.53$, $p < 0.001$, $n = 51$).

On the contrary, no positive relationships were found between the composition of peridinin-containing dinoflagellates as estimated by CHEMTAX and the SI values relative to *A. tamarense* culture calculated from $a_{ph}(\lambda)$ data and its second derivative (Spearman's rank correlation, Fig. 10e–f).

3.5. Similarity analysis of $a_{ph}(\lambda)$ derived from hyperspectral $R_{rs}(\lambda)$

The hyperspectral remote sensing reflectances ($R_{rs}(\lambda)$) measured in this study are depicted in Fig. 11. The spectral shapes and magnitudes of $R_{rs}(\lambda)$ varied considerably, indicating that various water types existed during each cruise. Comparisons of $a_{ph\_Rrs\text{-}derived}(\lambda)$ and $a_{ph\_Filter\text{-}pad}(\lambda)$ at several wavelengths showed a significant relationship for all wavelengths(Fig. 12a), and especially when excluding values of percentage difference (PD) over 100% (i.e., Stn. 6 in April 2010 and Stn. 9 in May 2011) (Fig. 12b). Root mean-square error (RMSE) values were low except for wavelengths over 547 nm (Fig. 12c). PD values within the 400–546 nm range between $a_{ph\_Filter\text{-}pad}(\lambda)$ and $a_{ph\_Rrs\text{-}derived}(\lambda)$ ranged from 5.3 to 180%, with an average of 32 ± 37%. An example of performance for the best case is shown in Fig. 12d. If PD values over 100% were excluded (i.e., Stn. 6 in April 2010 and Stn. 9 in May 2011), PD values from 5.3 to 52%, with an average of 22 ± 11%, were obtained. To better account for differences in spectral shape rather than in magnitude features in the derivative analysis, we normalized spectra of $a_{ph\_Filter\text{-}pad}(\lambda)$ and $a_{ph\_Rrs\text{-}derived}(\lambda)$ at 443 nm before comparison. PD values including the data from Stn. 6 in April 2010 and Stn. 9 in May 2011 showed a mean of 13 ± 6.2%. These results indicated that the inversion method of QAA well reproduced the spectral shape of $a_{ph}(\lambda)$. When estimating SI, as RMSE values were lower for

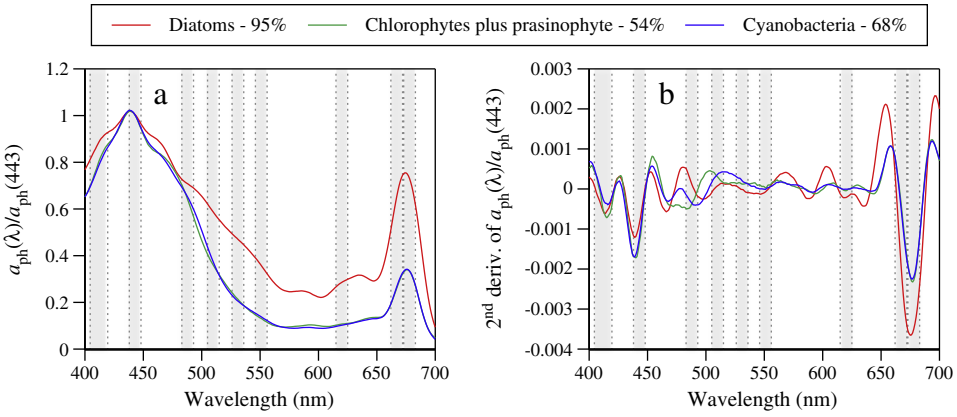

Fig. 8. Examples of the in situ (a) non- and (b) second derivative spectra of $a_{ph\_Filter\text{-}pad}(\lambda)/a_{ph\_Filter\text{-}pad}(443)$ with the predominance of diatoms, Chl *b*-containing phytoplankton, and cyanobacteria, as estimated by CHEMTAX. Gray frames with dashed lines represent the spectral locations of ocean color sensors in MODIS. The spectral bands at 510 nm and 620 nm of SeaWiFS and MERIS, respectively, are also overlaid.

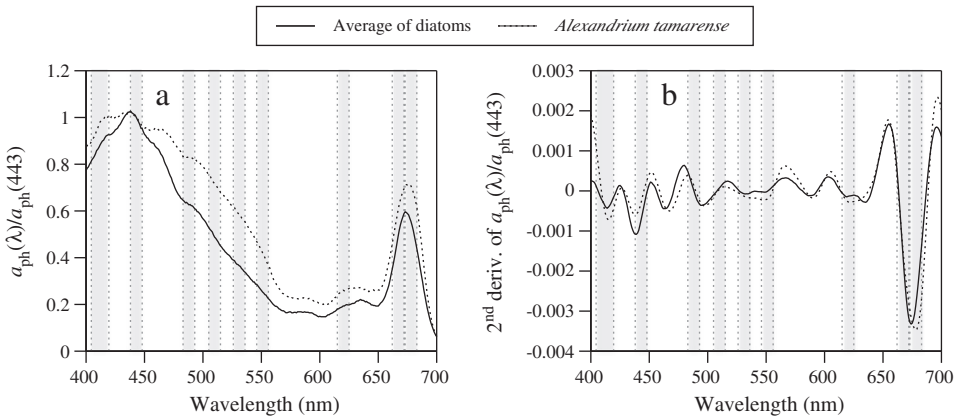

Fig. 9. Normalized absorption spectra ($a_{ph}(\lambda)/a_{ph}(443)$) and the second derivative spectra (2nd deriv. of $a_{ph}(\lambda)/a_{ph}(443)$) of the average of the three diatom cultures and the dinoflagellate culture (*Alexandrium tamarense*). Gray frames are as in Fig. 8.

$a_{ph\_Filter\text{-}pad}(\lambda)$ from 400 to 546 nm (Fig. 12c), the second derivative spectra of $a_{ph\_Rrs\text{-}derived}(\lambda)/a_{ph\_Rrs\text{-}derived}(443)$ were calculated within the range from 409 (=400 + 9) to 537 (=546 − 9) nm. Our results for SI relative to the average of the three diatom cultures had higher values at diatom-dominated stations (Cluster B), especially for second derivative spectra (Table 5), even the values obtained were lower than the ones using $a_{ph\_Filter\text{-}pad}(\lambda)$. A significant relationship between the SI values calculated from second derivative spectra and the composition of diatoms as estimated by CHEMTAX was found (Spearman's rank correlation, Fig. 13).

4. Discussion

4.1. The optical discrimination of phytoplankton groups by CHEMTAX and $a_{ph}(\lambda)$

CHEMTAX with HPLC phytoplankton pigment (Mackey et al., 1996) is a valuable tool for investigating whole phytoplankton communities, including the pico- and nano-phytoplankton groups, which are sometimes difficult to identify using light microscopy. Although CHEMTAX analysis has been successfully used in many investigations, one of the difficulties with this method is the choice of initial ratios of pigment:Chl *a* (Latasa, 2007; Mackey et al., 1996; Wright & Jeffrey, 2006). Therefore, it is important to carefully select and optimize the initial ratios of major phytoplankton groups (Mackey et al., 1996), especially in regions such as Funka Bay, for which no comparable data for HPLC pigments and initial ratios are available. To date, two main optimization procedures for the pigment:Chl *a* matrix have been proposed, one by Latasa (2007) and the other by Wright et al. (2009). The procedure of Latasa (2007) is a combination of different initial seed values and successive runs of CHEMTAX, and this method has been used in various waters (e.g., Eker-Develi et al., 2012; Latasa et al., 2010). However, using this method, it is difficult to observe a clear convergence in ratio values (Latasa et al., 2010). The procedure proposed by Wright et al. (2009) uses 61 CHEMTAX trials from randomized starting matrices and has similarly been used in different regions (e.g., Mendes et al., 2012; Schlüter, Henriksen, Nielsen, & Jakobsen, 2011). A combination of both procedures was exploited by Mendes et al. (2011) and de Souza, Mendes, Garcia, Pollery, and Brotas (2012). Kozlowski et al. (2011) evaluated the performance of both optimization procedures with a pigments dataset for the Antarctic coastal region. They showed subtle but non-significant differences between the methods of Latasa (2007) and of Wright et al. (2009).

In the present study, the randomized starting matrices of Wright et al. (2009) were used to estimate the optimal initial ratio. The obtained pigment:Chl *a* ratios were within the range summarized by Higgins et al. (2011) (Table 2). In terms of cluster tree based on HPLC pigments (Fig. 7), although two stations in Cluster A were separately clustered from Cluster B due to the different compositions of pigments (Table 3), the cophenetic index (*c*) indicated that cluster tree based on the CHEMTAX estimates showed good agreement with a reference cluster tree based on HPLC pigments, especially when considering data excluding two stations in Cluster A (i.e., Stns. 6 and 23 in April 2010, see Section 3.2). Seasonal variability in the composition of size-fractionated Chl *a* concentrations estimated by fluorometry showed the same trend as the results of CHEMTAX (see Section 3.2 and Fig. 5). Seasonal changes in phytoplankton community structure as estimated by CHEMTAX were consistent with previous studies. Previous studies with microscopy analysis in Funka Bay have reported that a diatom bloom occurred during spring in 1996 (Shinada et al., 1999), whereas cyanobacteria dominated during summer in 1988 (Odate, 1989). Odate, Yanada, Mizuta, and Maita (1993) reported the predominance of micro-sized (>10 μm) phytoplankton during the spring diatom bloom in Funka Bay in 1989. Dinoflagellates were not predominant over the study period. Although Tsunogai and Watanabe (1983) showed that dinoflagellates dominated after the spring diatom bloom of 1981, Kudo, Miyazono, Shimada, and Isoda (2005) and Miyazono, Nagai, Isao, and Tanizawa (2012) recently showed that a massive *A. tamarense* bloom started in the early 1960s and has continued until the late 1980s, but also that *A. tamarense* abundance has been declining since the 1990s.

Table 5
Average values of the similarity index (SI) relative to the average of three diatom cultures, and dinoflagellate culture (*A. tamarense*) for the non- (left side) and second (right side) derivative spectra of a filter-pad within the 400–700 nm range and R_{rs}-derived $a_{ph}(\lambda)/a_{ph}(443)$ within the 400–546 nm range in each cluster.

Cluster	Non-derivative spectra Mean ± SD	2nd derivative spectra Mean ± SD
SI values based on $a_{ph\_Filter\text{-}pad}(\lambda)$ relative to diatoms		
A	0.870 ± 0.012	0.832 ± 0.032
B	0.931 ± 0.029	0.825 ± 0.055
C	0.886 ± 0.012	0.677 ± 0.031
D	0.904 ± 0.024	0.713 ± 0.049
A. tamarense	0.925	0.755
SI values based on $a_{ph\_Filter\text{-}pad}(\lambda)$ relative to dinoflagellates (A. tamarense)		
A	0.818 ± 0.009	0.720 ± 0.007
B	0.878 ± 0.035	0.728 ± 0.055
C	0.832 ± 0.015	0.620 ± 0.026
D	0.850 ± 0.026	0.649 ± 0.039
SI values based on $a_{ph\_Rrs\text{-}derived}(\lambda)$ relative to diatoms		
A	0.948 ± 0.031	0.462 ± 0.125
B	0.956 ± 0.016	0.549 ± 0.075
C	0.921 ± 0.019	0.430 ± 0.033
D	0.913 ± 0.035	0.412 ± 0.042

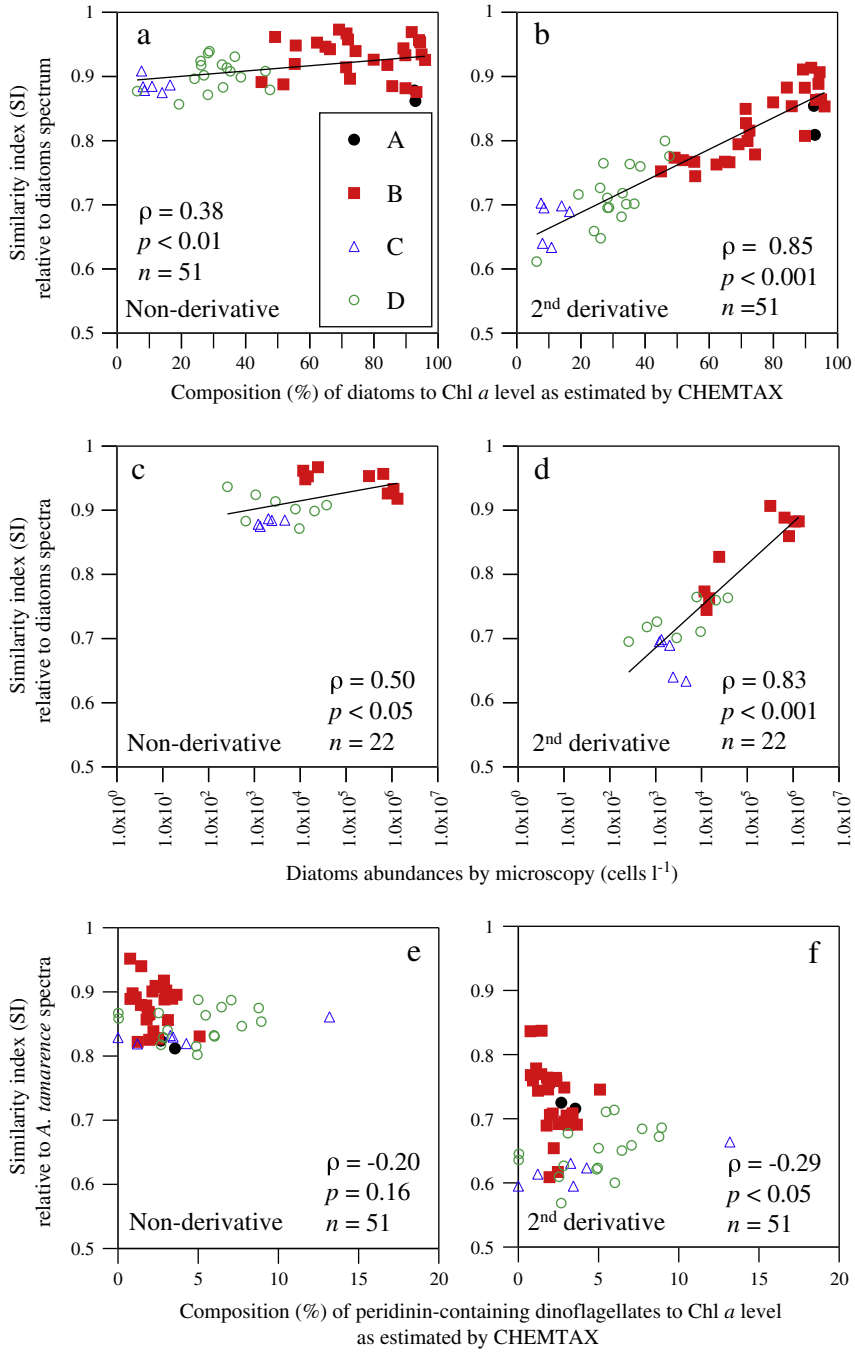

Fig. 10. Relationships between the similarity index (SI) relative to the average of three diatom cultures derived from the non- and second derivative spectra of $a_{ph}(\lambda)/a_{ph}(443)$ by filter-pad analysis using the range 400–700 nm and (a–b) the composition of diatoms as estimated by CHEMTAX, and (c–d) the cell densities of diatoms with microscopy, respectively. (e–f) Relationships between SI relative to *A. tamarense* cultures derived from the non- and second derivative spectra of $a_{ph}(\lambda)/a_{ph}(443)$ by filter-pad analysis using the range 400–700 nm and the composition of peridinin-containing dinoflagellates as estimated by CHEMTAX. Colors and symbols correspond to colors in HPLC pigments-based cluster groups A, B, C, and D (Fig. 7).

The cluster analysis was also performed based on hyperspectral optical data of $a_{ph\_Filter\text{-}pad}(\lambda)$. Subsequently, the *c* values of $a_{ph\_Filter\text{-}pad}(\lambda)$-based cluster tree relative to HPLC pigments- and CHEMTAX-based cluster trees were calculated (Table 4). Smaller *c* values were obtained compared with the *c* value between HPLC pigments- and CHEMTAX-based cluster trees, indicating that the seasonal changes in phytoplankton groups was more complicated to be assessed based on the cluster analysis of $a_{ph\_Filter\text{-}pad}(\lambda)$. However, higher *c* values were obtained when second derivative spectra of $a_{ph\_Filter\text{-}pad}(\lambda)$ were considered (Table 4). Therefore, once identified different water masses based on HPLC and CHEMTAX data, we employed a derivative spectroscopy/similarity index (SI) approach for $a_{ph\_Filter\text{-}pad}(\lambda)$ as an alternative method for identifying the dominant phytoplankton. This approach provides an optical detection technique for differentiating particular phytoplankton groups in mixed phytoplankton assemblages (Kirkpatrick et al., 2000; Millie et al., 1997). The results indicate that SI values relative to the average of the three diatom species using the second derivative spectra in clusters A and B were higher (Table 5). Furthermore, we found a strong relationship between the SI values calculated from second derivative spectra and the composition of diatoms as estimated by CHEMTAX (Fig. 10b). These results indicate that pigment and optical-based methods validate each other's performance and precision in estimating

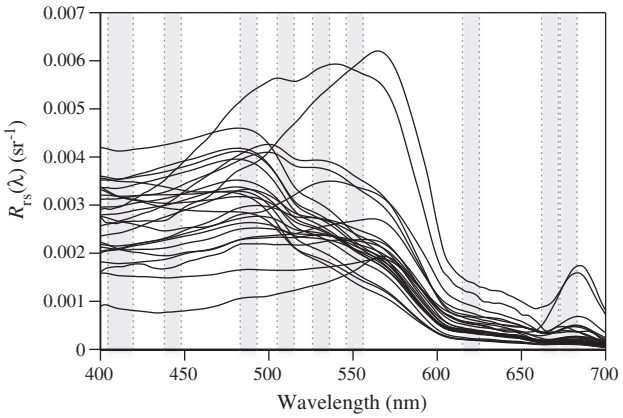

Fig. 11. Hyperspectral remote sensing reflectance ($R_{rs}(\lambda)$) derived from in situ radiometric measurements in this study. Gray frames are as in Fig. 8.

relative diatom abundance from bulk samples. Therefore, both SI values and CHEMTAX results have proven valuable to overcome the challenging task posed in this study. The derivative spectroscopy/SI approach for $a_{ph}(\lambda)$ in combination with CHEMTAX data as the reference for phytoplankton community structure has proven useful in improving understanding of phytoplankton community structure in the coastal waters of Funka Bay, in particular for those dominated by diatoms.

As represented by the results of the CHEMTAX and cluster analyses based on phytoplankton pigments, seasonal changes in the phytoplankton community structure in Funka Bay were mainly due to the succession of diatoms, Chl *b*-containing phytoplankton, and cyanobacteria (Figs. 5 and 7). Furthermore, SI values of the diatom-dominated clusters (Clusters A and B), relative to the average of the three diatom species estimated from the second derivatives, were significantly higher than those of the Chl *b*-containing phytoplankton- and cyanobacteria-dominated groups (Fig. 10 and Table 5). It is known that these three classes, which have distinct algal lineages, possess unique absorption spectra because of their different pigments: diatoms (red lineage) contain Chl *c* and fucoxanthin; cyanobacteria (prokaryote), zeaxanthin and phycobiliproteins; and chlorophytes and prasinophytes (green lineage), Chl *b* (Falkowski et al., 2004). These algal classes can be potentially discriminated by an optical absorption approach (Bissett et al., 2001; Schofield et al., 2004). In laboratory experiments with algal cultures, Millie, Schofield, Kirkpatrick, Johnsen, and Evens (2002) showed that the SI values of diatoms containing Chl *c* were different from those of Chl *b*-containing phytoplankton and cyanobacteria, meaning that the differential absorptions of these phytoplankton groups could be detectable using the derivative spectroscopy/SI approach. Accordingly, one of the main reasons for the significant relationship between diatom compositions as estimated by CHEMTAX and SI values (Fig. 10b) in this study could be the seasonal succession of diatoms, Chl *b*-containing phytoplankton, and cyanobacteria. These results suggested that it is possible to optically discriminate diatom-rich waters using a derivative spectroscopy/SI approach with bio-optical hyperspectral sensors (radiometers and spectrophotometers) on in situ mooring systems and satellites.

Since dinoflagellate, especially *A. tamarense*, cause scallop paralysis in Funka Bay (Miyazono et al., 2012), it is essential to identify the phytoplankton group in our study region. Nevertheless, in terms of peridinin-containing dinoflagellates, no positive relationships between the composition of dinoflagellates as estimated by CHEMTAX and SI

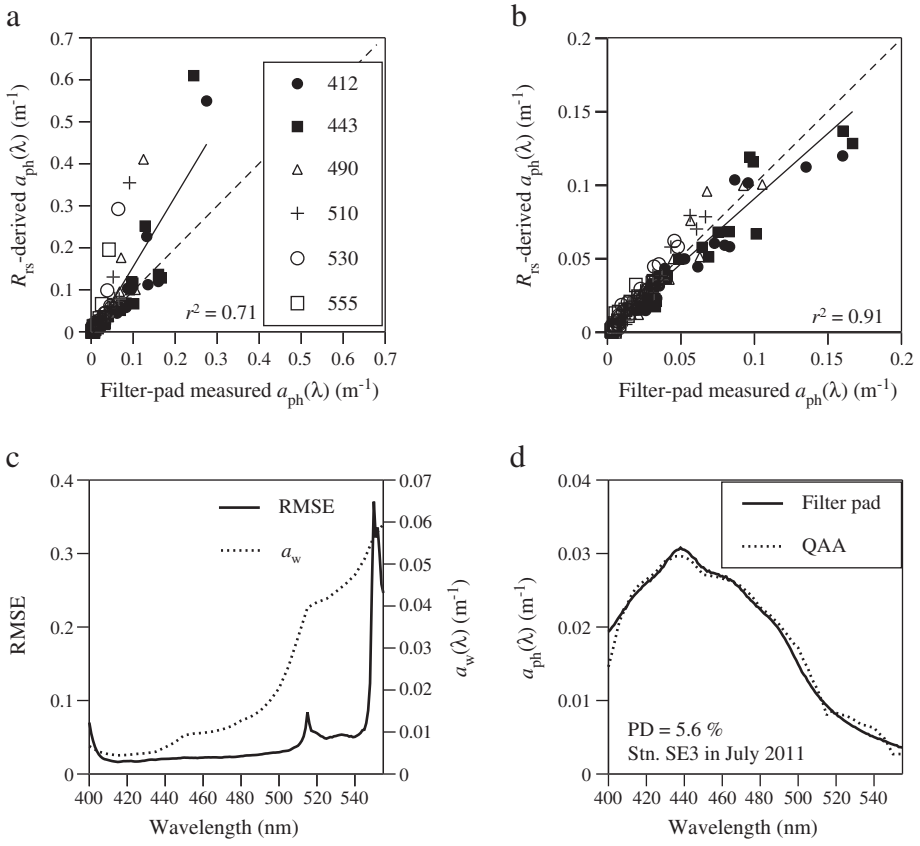

Fig. 12. Relationships between $a_{ph\_Filter\text{-}pad}(\lambda)$ and $a_{ph\_Rrs\text{-}derived}(\lambda)$ with QAA at some specific wavelengths for (a) all data and (b) data excluding percentage differences (PD) over 100%. Dashed lines in (a) and (b) represent 1:1 correlation. (c) Values of root mean square error (RMSE) between $a_{ph\_Filter\text{-}pad}(\lambda)$ and $a_{ph\_Rrs\text{-}derived}(\lambda)$ within 400–555 nm, and the absorption spectrum of water ($a_w(\lambda)$) (Pope & Fry, 1997). (d) Example of the comparison of $a_{ph\_Filter\text{-}pad}(\lambda)$ with $a_{ph\_Rrs\text{-}derived}(\lambda)$ within the 400–546 nm range for the minimum PD values at Stn. SE3 in July 2011.

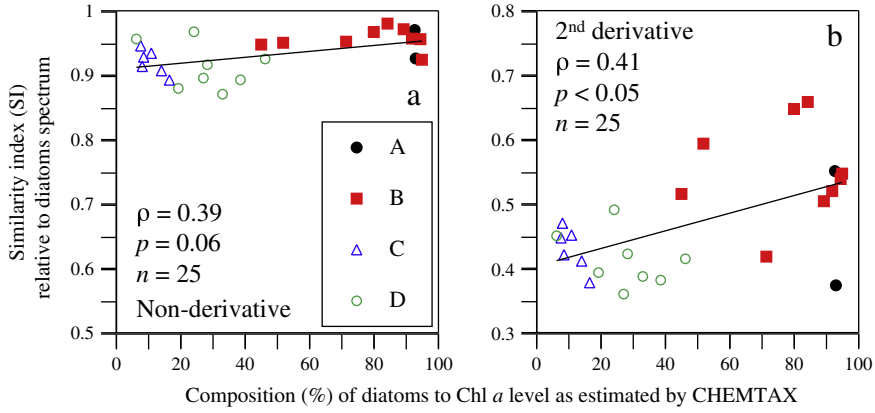

Fig. 13. Relationship between the composition of diatoms to Chl *a* concentration as estimated by CHEMTAX and the similarity index (SI) relative to the average of three diatom cultures derived from the (a) non- and (b) second derivative spectra of R_{rs}-derived $a_{ph}(\lambda)/a_{ph}(443)$. Colors in each symbol correspond to colors in cluster groups of A, B, C, and D in Fig. 7.

values relative to *A. tamarense* were found for any absorption spectra (Fig. 10e–f). Dinoflagellates were not predominant over the study period (Fig. 5), so the optical features of dinoflagellates did not account for a large fraction of the bulk absorption spectra. It has also been reported that *A. tamarense* contains mycosporine-like amino acids (MAAs) (Carreto, Carignan, & Montoya, 2001), which absorb the ultraviolet regions. Therefore, to optically identify *A. tamarense*, further studies are needed to investigate the absorption and reflectance due to MAAs, as in the investigation of Kahru and Mitchell (1998).

The pigment composition of phytoplankton varies widely with changes in irradiance (Laviale & Neveux, 2011) and micro- and macronutrients (Hopkinson et al., 2007). The absorption spectra of phytoplankton were also influenced by the package effect (Morel & Bricaud, 1981), cell-size composition (Ciotti et al., 2002), photoacclimation (Stæhr & Cullen, 2003), and changes in light (Johnsen & Sakshaug, 2007). The spectral shape of $a_{ph}(\lambda)$ depends on the physical condition of phytoplankton, which in turn influences the calculations of SI. In this study, exponentially growing cultures of diatoms and dinoflagellates were used. The dial cycle used for these cultures differs from that of summertime in Funka Bay (15:9 h light:dark). Therefore, further studies are needed to examine the influence of photoacclimation on SI estimations in natural mixed phytoplankton assemblages. Additionally, as we used only diatom and dinoflagellate cultures in this study, the method we developed should be validated for other phytoplankton groups and other locations.

4.2. Implications for ocean color remote sensing

The emergence of hyperspectral sensors (e.g., radiometers and spectrophotometers) has provided new opportunities to investigate phytoplankton dynamics in more detail. Several studies have shown the effectiveness of hyperspectral data for assessing phytoplankton pigment assemblages in coastal and open oceans (Lee & Carder, 2004; Torrecilla et al., 2011) and for detecting specific phytoplankton species or phytoplankton size structure both in the field (Craig et al., 2006; Lubac et al., 2008; Organelli et al., 2013) and in laboratory experiments with cultures (Mao et al., 2010). Furthermore, Bracher et al. (2009) developed the method for identifying cyanobacteria and diatoms (PhytoDOAS) from hyperspectral data of the Scanning Imaging Absorption Spectrometer for Atmospheric Chartography (SCIAMACHY) satellite sensor. Subsequently, Sadeghi et al. (2012) improved the PhytoDOAS method to allow coccolithophore bloom identification.

In this study, the derivative spectroscopy/SI approach described above was applied to hyperspectral $R_{rs}(\lambda)$-derived $a_{ph}(\lambda)$ estimated by QAA (Lee & Carder, 2004; Lee et al., 2009) to distinguish the dominance of diatoms from other phytoplankton. The results showed that SI values using the second derivative spectra were significantly correlated with the composition of diatoms (Fig. 13b). These results suggest that hyperspectral $R_{rs}(\lambda)$ with a derivative spectroscopy/SI approach could be a promising method for estimating the dominance of diatoms from in situ mooring systems and satellites. However, compared with in situ $a_{ph\_Filiter\text{-}pad}(\lambda)$ data (Fig. 10), $a_{ph}(\lambda)$ estimated from hyperspectral $R_{rs}(\lambda)$ was less precise. The visible range from 400 to 700 nm was used for the filter-pad analysis, and wavelengths over 547 nm were excluded from the hyperspectral analysis due to the absorption of water (Fig. 12).

To assess the effects of phytoplankton community structure on light absorption spectra, we examined correlations between the composition of diatoms, Chl *b*-containing phytoplankton (chlorophytes plus prasinophytes), and cyanobacteria as estimated by CHEMTAX and the in situ second derivative spectra (2^{nd} deriv. of $a_{ph\_Filter\text{-}pad}(\lambda)/a_{ph\_Filter\text{-}pad}(443)$) at each wavelength from 400 to 700 nm (Fig. 14). Interestingly, each phytoplankton group covered different regions of the visible light spectrum, including wavelengths over 547 nm. As phytoplankton composition switched from diatoms to Chl *b*-containing phytoplankton and then cyanobacteria, the high correlation with blue bands shifted toward longer or green bands. Variability in the spectral shapes reflected the presence of different pigments (i.e., Chl *c*, Chl *b*, and phycobiliprotein) among the phytoplankton groups. These features could contribute to the colorful niches of phytoplankton (Stomp,

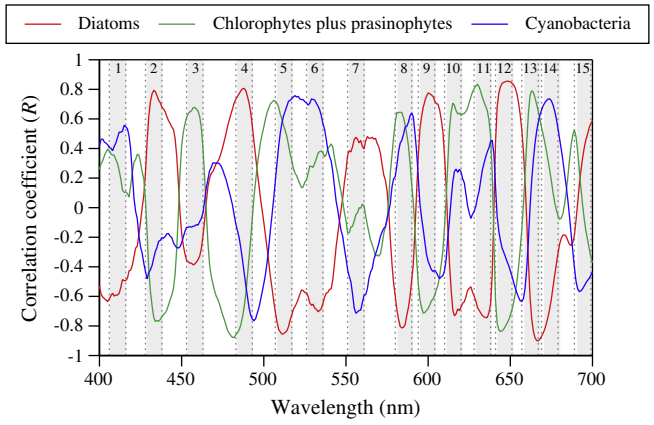

Fig. 14. Correlation coefficients (R) between the composition of diatoms, Chl *b*-containing phytoplankton (chlorophytes plus prasinophytes), and cyanobacteria as estimated by CHEMTAX and the in situ second derivative spectra of $a_{ph\_Filter\text{-}pad}(\lambda)/a_{ph\_Fulter\text{-}pad}(443)$ from 400 to 700 nm. Gray frames are the spectral bands recommended in this study (see Table 7).

Table 6
Results of a multiple linear regression analysis of CHEMTAX-derived Chl *a* concentrations in diatoms, Chl *b*-containing phytoplankton (chlorophytes plus prasinophytes), and cyanobacteria on $a_{ph\_Filter\text{-}pad}(\lambda)$ for a suite of three bands in the SeaWiFS, MODIS, and MERIS bands. Asterisks represent significance levels: *: $0.01 < p \leq 0.05$; **: $0.001 < p \leq 0.01$; ***: $p \leq 0.001$.

Phytoplankton	412 nm	443 nm	490 nm	510 nm	530 nm	555 nm	*R*
Diatoms	151***	−279***	264***				0.78
Chl *b* phytoplankton	−20.3***	30.0***	−13.6				0.70
Cyanobacteria	−1.67	0.91	1.83				0.17
Diatoms		−1.51	−133**	249***			0.80
Chl *b* phytoplankton		−7.12***	45.0***	−41.2***			0.84
Cyanobacteria		−2.10	8.51**	−6.11			0.22
Diatoms		10.4	−69.3		184***		0.79
Chl *b* phytoplankton		−9.12***	34.7***		−30.8***		0.82
Cyanobacteria		−2.43	7.34**		−5.22*		0.23
Diatoms			−256**	547**		−282	0.81
Chl *b* phytoplankton			60.2***	−108***		63**	0.82
Cyanobacteria			15.5*	−32.0		24.3	0.22
Diatoms			−74.4*		398	−263	0.79
Chl *b* phytoplankton			18.4***		−26.2	−4.15	0.74
Cyanobacteria			9.70***		−65.9***	74.4**	0.33

Huisman, Stal, & Matthijs, 2007). Second derivative spectra at 443 nm and 490 nm were positively correlated with diatom composition, but were negatively correlated with Chl *b*-containing phytoplankton. Recently, Lawrenz, Pinckney, Ranhofer, MacIntyre, and Richardson (2010) found co-variation in diatom and chlorophyte abundances with the spectral attenuation coefficient ($K_d(\lambda)$) in Winyah Bay, South Carolina, USA: chlorophytes showed positive relationships with ($K_d(442)$), while diatoms were negatively correlated with ($K_d(442)$). Furthermore, multiple linear regression analysis of the CHEMTAX-derived Chl *a* concentrations of these three algal classes on $a_{ph}(\lambda)$ for a suite of three bands in SeaWiFS and MODIS also revealed a shift from blue to green bands with changing phytoplankton groups (Table 6). Different slopes in the empirical ocean color chlorophyll algorithm for the SeaWiFS sensor (O'Reilly et al., 1998) are due to wavelength switching from the $R_{rs}(443)$ at low Chl *a* concentration, to $R_{rs}(490)$ at moderate Chl *a* concentration, and to $R_{rs}(510)$ at high Chl *a* concentration (e.g., Dierssen, 2010; Mao et al., 2010). Therefore, our results could account for the inverse relationship in these studies. Interestingly, 15 wavelengths showing high correlations with each phytoplankton community within the visible range cover the spectral bands of SeaWiFS, MODIS, and MERIS (Table 7 and Fig. 14). The bands presented in this study are similar to those proposed by Hoepffner and Sathyendranath (1991), who applied a Gaussian approach to decompose $a_{ph}(\lambda)$, and by Lee, Carder, Arnonr, and He (2007), who showed the 17 spectral bands required for ocean color sensors from a derivative analysis of hyperspectral $R_{rs}(\lambda)$. Additionally, Moline, Oliver, Bergmann, Glenn, and Schofield (2004) also showed the 25 useful wavelengths for detecting differences in phytoplankton by examining the relationship between the phytoplankton community and hyperspectral reflectance in coastal waters. Therefore, the 15 bands presented in Table 7 could be helpful in improving the estimation of phytoplankton community structure with multispectral optical data. However, according to IOCCG (2014), a recurrent problem in using ocean color data to extract information on phytoplankton is the limited number of wavelengths. IOCCG (2014) suggested that the development of hyperspectral sensor may make it possible for retrieving additional spectral features of phytoplankton communities that are indistinguishable though current multispectral sensors. In this sense, our results indicate that using hyperspectral optical data of $a_{ph}(\lambda)$ and $R_{rs}(\lambda)$ with derivative spectroscopy/SI approach is a promising approach to identify seasonal variability in the composition of diatoms in the coastal waters of Funka Bay. However, higher correlations were also found at wavelengths over 547 nm (Fig. 14). Recently, Aurin and Dierssen (2012) showed that the most successful semi-analytical model to retrieve inherent optical properties (IOPs) from ocean color remote sensing requires a red reflectance channel between 600 and 650 nm. Therefore, more accurate estimations of the dominance of diatoms by the derivative spectroscopy/SI approach are required for $a_{ph}(\lambda)$ at longer wavelengths.

Table 7
Summary of the spectral bands proposed by Hoepffner and Sathyendranath (1991), Lee et al. (2007), and this study, and channel positions used for ocean color sensors.

This study	Hoepffner and Sathyendranath (1991)	Lee et al. (2007)	SeaWiFS	MODIS	MERIS
	384	385			
		395			
411	413		412	412	413
		425			
433	435				
		440	443	443	443
458	461 (465)	460			
		475			
488	490	490	490	488	490
512		510	510		510
531	532			531	
		545			
556			555	551	
		565			560
585	583	580			
599					
615	623	615			620
633		635			
646	644				
	655				
662		665		667	665
674	676		670		
		685		678	681
694	700				
		710			709

5. Summary

In this study, we showed that the derivative spectroscopy/SI approach for hyperspectral $a_{ph}(\lambda)$ in combination with CHEMTAX analysis based on HPLC phytoplankton pigments as a reference for phytoplankton community structure is a valuable tool for estimating phytoplankton community structure and identifying the dominance of phytoplankton groups from bulk absorption in the coastal waters of Funka Bay. We also extended this method to hyperspectral remote sensing reflectance data and demonstrated that a hyperspectral optical

approach could be promising for monitoring phytoplankton groups when they are dominant. These results suggested that the combination of the derivative spectroscopy/SI approach for hyperspectral $a_{ph}(\lambda)$ and CHEMTAX analysis is helpful to develop methods for identifying phytoplankton functional groups from data obtained from in situ moored systems and satellites equipped with bio-optical hyperspectral sensors, and hence essential to improve our understanding of phytoplankton community structure. The real challenge of ocean color remote sensing is the identification of different groups of phytoplankton under non-bloom conditions (Nair et al., 2008). In this sense, our spectral-based approach has proven useful for detecting and monitoring seasonal changes of different phytoplankton groups in particular, for diatoms. However, this method should be validated for the assessment of other phytoplankton groups and for other regions. Furthermore, the estimation of $a_{ph}(\lambda)$ at longer wavelengths would be required for more accurate identification of phytoplankton groups from space, because remarkable differences in derivative spectra among phytoplankton groups were also found at wavelengths over 547 nm. Further studies are needed to investigate the relationship of IOPs and fluorescence (MacIntyre, Lawrenz, & Richardson, 2010) with phytoplankton community structure, and to develop a method for estimating IOPs at longer wavelengths.

Acknowledgments

We thank the captains and crews of T/S *Ushio* Maru and T/S *Oshoro* Maru. We are deeply grateful to the many post-doctoral researchers, technicians, and students in our laboratory, who helped us to collect samples during the cruises and gave us helpful comments on this paper. We are also most grateful to three anonymous reviewers for their constructive comments and suggestions on the manuscript. Our study was funded by the 'Hakodate Marine Bio Cluster Project' of the Ministry of Education, Culture, Sports, Science, and Technology program (0189) for fostering regional innovation, Japan.

References

Aguirre-gómez, R., Weeks, A.R., & Boxall, S.R. (2001). The identification of phytoplankton pigments from absorption spectra. *International Journal of Remote Sensing*, *22*, 315–338.

Alvain, S., Moulin, C., Dandonneau, Y., & Bréon, F.M. (2005). Remote sensing of phytoplankton groups in case 1 waters from global SeaWiFS imagery. *Deep-Sea Research Part I*, *52*, 1989–2004. http://dx.doi.org/10.1016/j.dsr.2005.06.015.

Armbrust, E.V. (2009). The life of diatoms in the world's oceans. *Nature*, *459*, 185–192. http://dx.doi.org/10.1038/nature08057.

Astoreca, R., Rousseau, V., Ruddick, K., Knechciak, C., Mol, B., Parent, J. -Y., et al. (2009). Development and application of an algorithm for detecting *Phaeocystis globosa* blooms in the case 2 Southern North Sea waters. *Journal of Plankton Research*, *31*, 287–300. http://dx.doi.org/10.1093/plankt/fbn116.

Aurin, D.A., & Dierssen, H.M. (2012). Advantages and limitations of ocean color remote sensing in CDOM-dominated, mineral-rich coastal and estuarine waters. *Remote Sensing of Environment*, *125*, 181–197. http://dx.doi.org/10.1016/j.rse.2012.07.001.

Austin, R.W. (1974). The remote sensing of spectral radiance from below the ocean surface. In N.G. Jerlov, & E.S. Nielsen (Eds.), *Optical aspects of oceanography* (pp. 317–343). Academic.

Baba, K., Sugawara, R., Nitta, H., Endou, K., & Miyazono, A. (2009). Relationship between spat density, food availability, and growth of spawners in cultured *Mizuhopecten yessoensis* in Funka Bay: Concurrence with ENSO. *Canadian Journal of Fisheries and Aquatic Sciences*, *66*, 6–17.

Babin, M., Cullen, J.J., Roesler, C.S., Donaghay, P.L., Doucette, G.J., Kahru, M., et al. (2005). New approaches and technologies for observing harmful algal blooms. *Oceanography*, *18*, 210–227.

Babin, M., Stramski, D., Ferrari, G.M., Claustre, H., Bricaud, A., Obolensky, G., et al. (2003). Variations in the light absorption coefficient of phytoplankton, nonalgal particles, and dissolved organic matter in coastal waters around Europe. *Journal of Geophysical Research*, *108*(C7), 3211. http://dx.doi.org/10.1029/2001JC000882.

Bidigare, R.R., Morrow, J.H., & Kiefer, D.A. (1989). Derivative analysis of spectral absorption by photosynthetic pigments in the western Sargasso Sea. *Journal of Marine Research*, *47*, 323–341.

Bidigare, R.R., van Heukelem, L., & Trees, C.C. (2005). Analysis of algal pigments by high-performance liquid chromatography. In R.A. Andersen (Ed.), *Algal culturing techniques* (pp. 327–345). Academic Press.

Bissett, W.P., Schofield, O., Glenn, S., Cullen, J.J., Miller, W.L., Pluddeman, A.J., et al. (2001). Resolving the impacts and feedbacks of ocean optics on upper ocean ecology. *Oceanography*, *14*, 30–53.

Bracher, A., Vountas, M., Dinter, T., Burrows, J.P., Röttgers, R., & Peeken, I. (2009). Quantitative observation of cyanobacteria and diatoms from space using PhytoDOAS on SCIAMACHY data. *Biogeosciences*, *6*, 751–764 (www.biogeosciences.net/6/751/2009/).

Bricaud, A., Claustre, H., Ras, J., & Oubelkheir, K. (2004). Natural variability of phytoplanktonic absorption in oceanic waters: Influence of the size structure of algal populations. *Journal of Geophysical Research*, *109*, C11010. http://dx.doi.org/10.1029/2004JC002419.

Butler, W.L., & Hopkins, D.W. (1970a). Higher derivative analysis of complex absorption spectra. *Photochemistry and Photobiology*, *12*, 439–450.

Butler, W.L., & Hopkins, D.W. (1970b). An analysis of fourth derivative spectra. *Photochemistry and Photobiology*, *12*, 451–456.

Carreto, J.I., Carignan, M.O., & Montoya, N.G. (2001). Comparative studies on mycosporine-like amino acids, paralytic shellfish toxins and pigment profiles of the toxic dinoflagellates *Alexandrium tamarense*, *A. catenella* and *A. minutum*. *Marine Ecology Progress Series*, *223*, 49–60.

Carteron, A., Jeanmougin, M., Leprieur, F., & Spatharis, S. (2012). Assessing the efficiency of clustering algorithms and goodness-of-fit measures using phytoplankton field data. *Ecological Informatics*, *9*, 64–68. http://dx.doi.org/10.1016/j.ecoinf.2012.03.008.

Chang, G., Mahoney, K., Briggs-Whitmire, A., Kohler, D., Mobley, C., Lewis, M., et al. (2004). The new age of hyperspectral oceanography. *Oceanography*, *17*, 22–29.

Chen, L.C. -M., Edelstein, T., & McLachlan, J. (1969). *Bonnemaisonia hamifera* hariot in nature and in culture. *Journal of Phycology*, *5*, 211–220.

Ciotti, Á. M., Lewis, M.R., & Cullen, J.J. (2002). Assessment of the relationships between dominant cell size in natural phytoplankton communities and the spectral shape of the absorption coefficient. *Limnology and Oceanography*, *47*, 404–417.

Cleveland, J.S., & Weidemann, A.D. (1993). Quantifying absorption by aquatic particles: A multiple scattering correction for glass-fiber filters. *Limnology and Oceanography*, *38*, 1321–1327.

Craig, S.E., Lohrenz, S.E., Lee, Z., Mahoney, K.L., Kirkpatrick, G.J., Schofield, O.M., et al. (2006). Use of hyperspectral remote sensing reflectance for detection and assessment of the harmful alga, *Karenia brevis*. *Applied Optics*, *45*, 5414–5425.

Cullen, J.J., Ciotti, Á. M., Davis, R.F., & Lewis, M.R. (1997). Optical detection and assessment of algal blooms. *Limnology and Oceanography*, *45*, 1223–1239.

de Souza, M.S., Mendes, C.R.B., Garcia, V.M.T., Pollery, R., & Brotas, V. (2012). Phytoplankton community during a coccolithophorid bloom in the Patagonian Shelf: Microscopic and high-performance liquid chromatography pigment analyses. *Journal of the Marine Biological Association of the United Kingdom*, *92*, 13–27. http://dx.doi.org/10.1017/S0025315411000439.

Devred, E., Turpie, K.R., Moses, W., Klemas, V.V., Moisan, T., Babin, M., et al. (2013). Future retrievals of water column bio-optical properties using the Hyperspectral Infrared Imager (HyspIRI). *Remote Sensing*, *5*, 6812–6837. http://dx.doi.org/10.3390/rs5126812.

Dierssen, H.M. (2010). Perspectives on empirical approaches for ocean color remote sensing of chlorophyll in a changing climate. *Proceedings of the National Academy of Sciences of the United States of America*, *107*(40), 17073–17078. http://dx.doi.org/10.1073/pnas.0913800107.

Dierssen, H.M., Zimmerman, R.C., Drake, L.A., & Burdige, D. (2010). Benthic ecology from space: Optics and net primary production in seagrass and benthic algae across the Great Bahama Bank. *Marine Ecology Progress Series*, *411*, 1–15. http://dx.doi.org/10.3354/meps08665.

Eker-Develi, E., Berthon, J. -F., Canuti, E., Slabakova, N., Moncheva, S., Shtereva, G., et al. (2012). Phytoplankton taxonomy based on CHEMTAX and microscopy in the northwestern Black Sea. *Journal of Marine Systems*, *94*, 18–32. http://dx.doi.org/10.1016/j.jmarsys.2011.10.005.

Falkowski, P.G., Barber, R.T., & Smetcek, V. (1998). Biogeochemical controls and feedbacks on ocean primary production. *Science*, *281*, 200–206. http://dx.doi.org/10.1126/science.281.5374.200.

Falkowski, P.G., Katz, M.E., Knoll, A.H., Quigg, A., Raven, J.A., Schofield, O., et al. (2004). The evolution of modern eukaryotic phytoplankton. *Science*, *305*, 354–360. http://dx.doi.org/10.1126/science.1095964.

Faust, M.A., & Norris, K.H. (1985). In vivo spectrophotometric analysis of photosynthetic pigments in natural populations of phytoplankton. *Limnology and Oceanography*, *30*, 1316–1322.

Fujiki, T., & Taguchi, S. (2002). Variability in chlorophyll a specific absorption coefficient in marine phytoplankton as a function of cell size and irradiance. *Journal of Plankton Research*, *24*, 859–874.

Hashihama, F., Horimoto, N., Kanda, J., Furuya, K., Ishimaru, T., & Saino, T. (2008). Temporal variation in phytoplankton composition related to water mass properties in the central part of Sagami bay. *Journal of Oceanography*, *64*, 23–37.

Hashimoto, S., Ueno, K., Takahashi, K., Suzuki, T., & Itabashi, Y. (2010). Photosensitivity in mice caused by pyropheophorbide in the midgut gland of the scallop *Patinopecten yessoensis* observed in diarrhetic shellfish poisoning mouse bioassays. *Fisheries Science*, *76*, 529–536. http://dx.doi.org/10.1007/s12562-010-0233-7.

Higgins, H., Wright, S.W., & Schlüter, L. (2011). Quantitative interpretation of chemotaxonomic pigment data. In S. Roy, C. Llewellyn, E.S. Egeland, & G. Johnsen (Eds.), *Phytoplankton pigments: Characterization, chemotaxonomy and applications in oceanography* (pp. 257–313). Cambridge, UK: Cambridge University Press.

Hirata, T., Hardman-Mountford, N.J., Brewin, R.J.W., Aiken, J., Barlow, R., Suzuki, K., et al. (2011). Synoptic relationships between surface chlorophyll-*a* and diagnostic pigments specific to phytoplankton functional types. *Biogeosciences*, *8*, 311–327. http://dx.doi.org/10.5194/bg-8-311-2011.

Hirawake, T., Shinmyo, K., Fujiwara, A., & Saitoh, S. -I. (2012). Satellite remote sensing of primary productivity in the Bering and Chukchi Seas using a absorption-based approach. *ICES Journal of Marine Science*, *69*, 1194–1204.

Hoepffner, N., & Sathyendranath, S. (1991). Effect of pigment composition on absorption properties of phytoplankton. *Marine Ecology Progress Series*, *73*, 11–23.

Hopkinson, B.M., Mitchell, B.G., Reynolds, R.A., Wang, H., Selph, K.E., Measures, C.I., et al. (2007). Iron limitation across chlorophyll gradients in the southern Drake Passage: Phytoplankton responses to iron addition and photosynthetic indicators of iron stress. *Limnology and Oceanography*, *52*, 2540–2554.

Hornik, K. (2012). Clue: Cluster ensembles. R package version 0.3-45. URL http://CRAN.R-project.org/package=clue

Imai, I., Itakura, S., Matsuyama, Y., & Yamaguchi, M. (1996). Selenium requirement for growth of a novel red tide flagellate *Chattonella verruculosa* (Raphidophyceae) in culture. *Fisheries Science*, *62*, 834–835.

Imai, I., Yamaguchi, M., & Hori, Y. (2006). Eutrophication and occurrence of harmful algal blooms in the Seto Island Sea, Japan. *Plankton & Benthos Research*, *1*, 71–84.

IOCCG (2014). Phytoplankton functional types from space. In Shubha Sathyendranath (Ed.), *Reports of the International Ocean-Colour Coordinating Group, No. 15*.

Isada, T., Iida, T., Liu, H., Saitoh, S. -I., Nishioka, J., Nakatsuka, T., et al. (2013). Influence of Amur River discharge on phytoplankton photophysiology in the Sea of Okhotsk during late summer. *Journal of Geophysical Research*, *118*, 1995–2013. http://dx.doi.org/10.1002/jgrc.20159.

Isada, T., Kuwata, A., Saito, H., Ono, T., Ishii, M., Yoshikawa-Inoue, H., et al. (2009). Photosynthetic features and primary productivity of phytoplankton in the Oyashio and Kuroshio–Oyashio transition regions of the northwest Pacific. *Journal of Plankton Research*, *31*, 1009–1025. http://dx.doi.org/10.1093/plankt/fbp050.

Johnsen, G., & Sakshaug, E. (2007). Biooptical characteristics of PSII and PSI in 33 species (13 pigment groups) of marine phytoplankton, and the relevance for pulse-amplitude-modulated and fast-repetition-rate fluorometry. *Journal of Phycology*, *43*, 1236–1251. http://dx.doi.org/10.1111/j.1529-8817.2007.00422.x.

Kahru, M., & Mitchell, B.G. (1998). Spectral reflectance and absorption of a massive red tide off southern California. *Journal of Geophysical Research*, *103*, 21601–21609.

Kirkpatrick, G.J., Millie, D.F., Moline, M.A., & Schofield, O. (2000). Optical discrimination of a phytoplankton species in natural mixed populations. *Limnology and Oceanography*, *45*, 467–471.

Kishino, M., Takahashi, M., Okami, N., & Ichimura, S. (1985). Estimation of the spectral absorption coefficients of phytoplankton in the sea. *Bulletin of Marine Science*, *37*, 634–642.

Kozlowski, W.A., Deutschman, D., Garibotti, I., Trees, C., & Vernet, M. (2011). An evaluation of the application of CHEMTAX to Antarctic coastal pigment data. *Deep-Sea Research Part I*, *58*, 350–364. http://dx.doi.org/10.1016/j.dsr.2011.01.008.

Kudo, I., Miyazono, A., Shimada, H., & Isoda, Y. (2005). The lower trophic ecosystem in Funka Bay and its long-term monitoring index. *Bulletin on Coastal Oceanography*, *43*, 33–38 (in Japanese with English abstract).

Kuroda, H., Isoda, Y., Takeoka, H., Kuma, K., Honda, S., Matsuura, H., et al. (2012). Intrusion of the Oyashio water into the eastern mouth of Tsugaru Strait in early summer, 2003. *Continental Shelf Research*, *32*, 36–46.

Latasa, M. (2007). Improving estimations of phytoplankton class abundance using CHEMTAX. *Marine Ecology Progress Series*, *329*, 13–21.

Latasa, M., Scharek, R., Vidal, M., Vila-Reixach, G., Gutiérrez-Rodríguez, A., Emelianov, M., et al. (2010). Preferences of phytoplankton groups for waters of different trophic status in the northwestern Mediterranean Sea. *Marine Ecology Progress Series*, *407*, 27–42. http://dx.doi.org/10.3354/meps08559.

Laviale, M., & Neveux, J. (2011). Relationships between pigment ratios and growth irradiance in 11 marine phytoplankton species. *Marine Ecology Progress Series*, *425*, 64–77. http://dx.doi.org/10.3354/meps09013.

Lawrenz, E.J., Pinckney, L., Ranhofer, M.L., MacIntyre, H.L., & Richardson, T.L. (2010). Spectral irradiance and phytoplankton community composition in a blackwater-dominated estuary, Winyah Bay, South Carolina, USA. *Estuaries and Coasts*, *33*, 1186–1201. http://dx.doi.org/10.1007/s12237-010-9310-5.

Lee, Z., & Carder, K.L. (2004). Absorption spectrum of phytoplankton pigments derived from hyperspectral remote-sensing reflectance. *Remote Sensing of Environment*, *89*, 361–368.

Lee, Z., Carder, K.L., Arnonr, R., & He, M. (2007). Determination of primary spectral bands for remote sensing of aquatic environments. *Sensors*, *7*, 3428–3441.

Lee, Z., Lubac, B., Werdell, J., & Arnone, R. (2009). An update of the quasi-analytical algorithm (QAA_v5). http://www.ioccg.org/groups/software.html

Llewellyn, C.A., Fishwick, J.R., & Blackford, J.C. (2005). Phytoplankton community assemblage in the English Channel: A comparison using chlorophyll *a* derived from HPLC-CHEMTAX and carbon derived from microscopy cell counts. *Journal of Plankton Research*, *27*, 103–119. http://dx.doi.org/10.1093/plankt/fbh158.

Louchard, E.M., Reid, R.P., Stephens, C.F., Davis, C.O., Leathers, R.A., Downes, T.V., et al. (2002). Derivative analysis of absorption features in hyperspectral remote sensing data of carbonate sediments. *Optics Express*, *10*, 1573–1584.

Lubac, B., Loisel, H., Guiselin, N., Astoreca, R., Artigas, L.F., & Mériaux, X. (2008). Hyperspectral and multispectral ocean color inversions to detect *Phaeocystis globosa* blooms in coastal waters. *Journal of Geophysical Research*, *113*, C06026. http://dx.doi.org/10.1029/2007JC004451.

MacIntyre, H.L., Lawrenz, E., & Richardson, T. (2010). Taxonomic discrimination of phytoplankton by spectral fluorescence. In D.J. Sugget, O. Prášil, & M.A. Borowitzka (Eds.), *Chlorophyll a fluorescence in aquatic science* (pp. 129–169). Springer.

Mackey, M.D., Mackey, D.J., Higgins, H.W., & Wright, S.W. (1996). CHEMTAX — program for estimating class abundances from chemical markers: Application to HPLC measurements of phytoplankton. *Marine Ecology Progress Series*, *144*, 265–283.

Mao, Z., Stuart, V., Pan, D., Chen, J., Gong, F., Huang, H., et al. (2010). Effects of phytoplankton species composition on absorption spectra and modeled hyperspectral reflectance. *Ecological Informatics*, *5*, 359–366. http://dx.doi.org/10.1016/j.ecoinf.2010.04.004.

Marra, J., Trees, C.C., & O'Reilly, J.E. (2007). Phytoplankton pigment absorption: A strong predictor of primary productivity in the surface ocean. *Deep-Sea Research Part I*, *54*, 155–163. http://dx.doi.org/10.1016/j.dsr.2006.12.001.

Matsuoka, A., Larouche, P., Poulin, M., Vincent, W., & Hattori, H. (2009). Phytoplankton community adaptation to changing light levels in the southern Beaufort Sea, Canadian Arctic. *Estuarine, Coastal and Shelf Science*, *82*, 537–546.

Mendes, C.R., de Souza, M.S., Garcia, V.M.T., Leal, M.C., Brotas, V., & Garcia, C.A.E. (2012). Dynamics of phytoplankton communities during late summer around the tip of the Antarctic Peninsula. *Deep-Sea Research Part I*, *65*, 1–14. http://dx.doi.org/10.1016/j.dsr.2012.03.002.

Mendes, C.R., Sá, C., Vitorino, J., Borges, C., Garcia, V.M.T., & Brotas, V. (2011). Spatial distribution of phytoplankton assemblages in the Nazaré submarine canyon region (Portugal): HPLC-CHEMTAX approach. *Journal of Marine Systems*, *87*, 90–101. http://dx.doi.org/10.1016/j.jmarsys.2011.03.005.

Mérigot, B., Durbec, J. -P., & Gaertner, J. -C. (2010). On goodness-of-fit measure for dendrogram-based analyses. *Ecology*, *91*, 1850–1859.

Meyer, D., & Buchta, C. (2012). Proxy: Distance and similarity measures. R package version 0.4-9. URL http://CRAN.R-project.org/package=proxy

Millie, D.F., Kirkpatrick, G.J., & Vinyard, B.T. (1995). Relating photosynthetic pigments and in vivo optical density spectra to irradiance for the Florida red-tide dinoflagellate *Gymnodinium breve*. *Marine Ecology Progress Series*, *120*, 65–75.

Millie, D.F., Schofield, O.M., Kirkpatrick, G.J., Johnsen, G., & Evens, T.J. (2002). Using absorbance and fluorescence spectra to discriminate microalgae. *European Journal of Phycology*, *37*, 313–322.

Millie, D.F., Schofield, O.M., Kirkpatrick, G.J., Johnsen, G., Tester, P.A., & Vinyard, B.T. (1997). Detection of harmful algal blooms using photopigments and absorption signatures: A case study of the Florida red tide dinoflagellate, *Gymnodinium breve*. *Limnology and Oceanography*, *42*, 1240–1251.

Miyake, H., Tanaka, I., & Murakami, T. (1988). Outflow of water from Funka Bay, Hokkaido, during early spring. *Journal of the Oceanographical Society of Japan*, *44*, 163–170.

Miyazono, A., Nagai, S., Isao, K., & Tanizawa, K. (2012). Viability of *Alexandrium tamarense* cysts in the sediment of Funka Bay, Hokkaido, Japan: Over a hundred year survival times for cysts. *Harmful Algae*, *16*, 81–88. http://dx.doi.org/10.1016/j.hal.2012.02.001.

Moline, M.A., Oliver, M.J., Bergmann, T., Glenn, S., & Schofield, O.M.E. (2004). Episodic physical forcing and the structure of phytoplankton communities in the coastal waters of New Jersey. *Journal of Geophysical Research*, *109*, C12S05. http://dx.doi.org/10.1029/2003JC001985.

Morel, A., & Bricaud, A. (1981). Theoretical results concerning light absorption in a discrete medium, and application to specific absorption of phytoplankton. *Deep-Sea Research*, *28A*, 1375–1393.

Mueller, J.L., Fargion, G.S., & McClain, C.R. (2003). Radiometric measurements and data analysis protocols. In ocean optics protocols for satellite ocean color sensor validation. *Revision 4, Volume III, NASA/TM-2003-211621/Rev4-Vol. III*. Greenbelt, Maryland: NASA Goddard Space Flight Center.

Nair, A., Sathyendranath, S., Platt, T., Morales, J., Stuart, V., Forget, M. -H., et al. (2008). Remote sensing of phytoplankton functional types. *Remote Sensing of Environment*, *112*, 2266–3375. http://dx.doi.org/10.1016/j.rse.2008.01.021.

Nakada, S., Ishikawa, Y., Awaji, T., In, T., Koyamada, K., Watanobe, M., et al. (2013). An integrated approach to the heat and water mass dynamics of a large bay: High-resolution simulations of Funka Bay, Japan. *Journal of Geophysical Research*, *118*, 3530–3547. http://dx.doi.org/10.1002/jgrc.20262.

O'Reilly, J.E., Maritorena, S., Mitchell, B.G., Siegel, D.A., Carder, K.L., Garver, S.A., et al. (1998). Ocean color chlorophyll algorithms for SeaWiFS. *Journal of Geophysical Research*, *103C*, 24937–24953.

Odate, T. (1989). Seasonal changes in cell density of cyanobacteria and other picophytoplankton populations in Funka Bay, Japan. *Bulletin of Plankton Society of Japan*, *36*, 53–61.

Odate, T., Yanada, M., Mizuta, H., & Maita, Y. (1993). Phytoplankton carbon biomass estimated from the size-fractionated chlorophyll *a* concentration and cell density in the northern coastal waters from spring bloom to summer. *Bulletin of Plankton Society of Japan*, *39*, 127–144.

Organelli, E., Bricaud, A., Antoine, D., & Uitz, J. (2013). Multivariate approach for the retrieval of phytoplankton size structure from measured light absorption spectra in the Mediterranean Sea (BOUSSOLE site). *Applied Optics*, *52*(11), 2257–2273.

Pan, X., Mannino, A., Marshall, H.G., Filippino, K.C., & Mulholland, M.R. (2011). Remote sensing of phytoplankton community composition along the northeast of the United States. *Remote Sensing of Environment*, *115*, 3731–3747. http://dx.doi.org/10.1016/j.rse.2011.09.011.

Pan, X., Mannino, A., Russ, M.E., Hooker, S.B., & Harding, L.W., Jr. (2010). Remote sensing of phytoplankton pigment distribution in the United States northeast coast. *Remote Sensing of Environment*, *114*, 2403–2416. http://dx.doi.org/10.1016/j.rse.2010.05.015.

Pope, R.M., & Fry, E.S. (1997). Absorption spectrum (380–700 nm) of pure water. II. Integrating cavity measurements. *Applied Optics*, *36*, 8710–8723.

Richardson, T.L., & Jackson, G.A. (2007). Small phytoplankton and carbon export from the surface ocean. *Science*, *315*, 838–840. http://dx.doi.org/10.1126/science.1133471.

Ryan, J.P., Davis, C.O., Tufillaro, N.B., Kudela, R.M., & Gao, B. -C. (2014). Application of the Hyperspectral Imager for the Coastal Ocean to phytoplankton ecology studies in Monterey Bay, CA, USA. *Remote Sensing*, *6*, 1007–1025. http://dx.doi.org/10.3390/rs6021007.

Sadeghi, A., Dinter, T., Vountas, M., Taylor, B.B., Altenburg-Soppa, M., Peeken, I., et al. (2012). Improvement to the PhytoDOAS method for identification of coccolithophores using hyper-spectral satellite data. *Ocean Science*, *8*, 1055–1070. http://dx.doi.org/10.5194/os-8-1055-2012.

Sasaki, H., Miyamura, T., Saitoh, S. -I., & Ishizaka, J. (2005). Seasonal variation of absorption by particles and colored dissolved organic matter (CDOM) in Funka Bay, southwestern Hokkaido, Japan. *Estuarine, Coastal and Shelf Science*, *64*, 447–458.

Sathyendranath, S., Stuart, V., Platt, T., Bouman, H., Ulloa, O., & Maass, H. (2005). Remote sensing of ocean colour: Towards algorithm for retrieval of pigment composition. *Indian Journal of Marine Sciences*, *33*, 333–340.

Schlüter, L., Henriksen, P., Nielsen, T.G., & Jakobsen, H.H. (2011). Phytoplankton composition and biomass across the southern Indian Ocean. *Deep-Sea Research Part I*, *58*, 546–556. http://dx.doi.org/10.1016/j.dsr.2011.02.007.

Schofield, O., Bergmann, T., Oliver, M.J., Irwin, A., Kirkpatrick, G., Bissett, W.P., et al. (2004). Inversion of spectral absorption in the optically complex coastal waters of the Mid-Atlantic Bight. *Journal of Geophysical Research*, *109*, C12S04. http://dx.doi.org/10.1029/2003JC002071.

Schofield, O.M., Grzymski, J., Bissett, W.P., Kirkpatrick, G.J., Millie, D.F., Moline, M., et al. (1999). Optical monitoring and forecasting systems for harmful algal blooms: Possibility or pipe dream? *Journal of Phycology*, *35*, 1477–1496.

Shinada, A., Shiga, N., & Ban, S. (1999). Origin of *Thalassiosira* diatoms that cause the spring phytoplankton bloom in Funka Bay, southwestern Hokkaido, Japan. *Plankton Biology and Ecology*, *46*, 89–93.

Smith, C.M., & Alberte, R.S. (1994). Characterization of in vivo absorption features of chlorophytes, phaeophyte and rhodophyte algal species. *Marine Biology*, *118*, 511–521.

Stæhr, P.A., & Cullen, J.J. (2003). Detection of *Karenia mikimotoi* by spectral absorption signatures. *Journal of Plankton Research*, *25*, 1237–1249. http://dx.doi.org/10.1093/plankt/fbg083.

Stomp, M., Huisman, J.L., Stal, J., & Matthijs, H.C.P. (2007). Colorful niches of phototrophic microorganisms shaped by vibrations of the water molecule. *The ISME Journal*, *1*, 271–282. http://dx.doi.org/10.1038/ismej.2007.59.

Stramski, D., Reynolds, R.A., Babin, M., Kaczmarek, S., Lewis, M.R., Röttgers, R., et al. (2008). Relationships between the surface concentration of particulate organic carbon and optical properties in the eastern South Pacific and eastern Atlantic Oceans. *Biogeosciences*, *5*, 171–201 (www.biogeosciences.net/5/171/2008/).

Suzuki, K., Hinuma, A., Saito, H., Kiyosawa, H., Liu, H., Saino, T., et al. (2005). Responses of phytoplankton and heterotrophic bacteria in the northwest subarctic Pacific to in situ iron fertilization as estimated by HPLC pigment analysis and flow cytometry. *Progress in Oceanography*, *64*, 167–187. http://dx.doi.org/10.1016/j.pocean.2005.02.007.

Suzuki, R., & Ishimaru, T. (1990). An improved method for the determination of phytoplankton chlorophyll using N, N-dimethylformamide. *Journal of Oceanography*, *46*, 190–194.

Tassan, S., & Ferrari, G.M. (1995). An alternative approach to absorption measurements of aquatic particles retained on filters. *Limnology and Oceanography*, *40*, 1358–1368.

Taylor, B.B., Torrecilla, E., Bernhardt, A., Taylor, M.H., Peeken, I., Röttgers, R., et al. (2011). Bio-optical provinces in the eastern Atlantic Ocean and their biogeographical relevance. *Biogeosciences*, *8*, 3609–3629. http://dx.doi.org/10.5194/bg-8-3609-2011.

Tomas, C.R. (1997). *Identifying marine phytoplankton*. San Diego, USA: Academic Press.

Torrecilla, E., Stramski, D., Reynolds, R.A., Millán-Núñez, E., & Piera, J. (2011). Cluster analysis of hyperspectral optical data for discriminating phytoplankton pigment assemblages in the open ocean. *Remote Sensing of Environment*, *115*, 2578–2593. http://dx.doi.org/10.1016/j.rse.2011.05.014.

Tsai, F., & Philpot, W. (1998). Derivative analysis of hyperspectral data. *Remote Sensing of Environment*, *66*, 41–51.

Tsunogai, S., & Watanabe, Y. (1983). Role of dissolved silicate in the Occurrence of a phytoplankton bloom. *Journal of the Oceanographical Society of Japan*, *39*, 231–239.

Van Heukelem, L., & Thomas, C.S. (2001). Computer-assisted high-performance liquid chromatography method development with applications to the isolation and analysis of phytoplankton pigments. *Journal of Chromatography A*, *910*, 31–49.

Veldhuis, M.J.W., & Kraay, G.W. (2004). Phytoplankton in the subtropical Atlantic Ocean: Towards a better assessment of biomass and composition. *Deep-Sea Research Part I*, *51*, 507–530.

Welschmeyer, N.A. (1994). Fluorometric analysis of chlorophyll-*a* in the presence of chlorophyll-*b* and phaeopigments. *Limnology and Oceanography*, *39*, 1985–1992.

Wright, S.W., Ishikawa, A., Marchant, H.J., Davidson, A.T., van den Enden, R.L., & Nash, G.V. (2009). Composition and significance of picophytoplankton in Antarctic waters. *Polar Biology*, *32*, 797–808. http://dx.doi.org/10.1007/s00300-009-0582-9.

Wright, S.W., & Jeffrey, S.W. (2006). Pigment markers for phytoplankton production. In John K. Volkman (Ed.), *Marine organic matter, biomarkers, isotopes and DNA series. The handbook of environmental chemistry. Reactions and Processes, Part N, vol. 2*. (pp. 71–104). Springer-Verlag.

Zapata, M., Fraga, S., Rodríguez, F., & Garrido, J.L. (2012). Pigment-based chloroplast types in dinoflagellates. *Marine Ecology Progress Series*, *465*, 33–52. http://dx.doi.org/10.3354/meps09879.

Zapata, M., Jeffrey, S.W., Wright, S.W., Rodríguez, F., Garrido, J.L., & Clementson, L. (2004). Photosynthetic pigments in 37 species (65 strains) of Haptophyta: Implications for oceanography and chemotaxonomy. *Marine Ecology Progress Series*, *270*, 83–102.